Title

Rapid Estimation of the State-of-Health (SoH) of a Battery Pack Consisting of Four Cells Connected in Series

Author

Landore, Shantanu

Publication Date

2022

Peer reviewed|Thesis/dissertation

Rapid Estimation of the State-of-Health (SoH) of a Battery Pack Consisting of Four Cells Connected in Series

By

SHANTANU LANDORE

THESIS

Submitted in partial satisfaction of the requirements for the degree of

MASTER OF SCIENCE

in

Mechanical and Aerospace Engineering

in the

OFFICE OF GRADUATE STUDIES

of the

UNIVERSITY OF CALIFORNIA

DAVIS

Approved:

Jae Wan Park, Chair

Bryan M Jenkins

Alan T Jenn

Committee in Charge

2022

Abstract

Lithium-ion batteries are widely used in the Electric Vehicle (EV) and the Energy Storage Systems (ESS) applications. In such systems, the batteries are connected in combinations of series and parallel connections in such a way that the overall current and voltage of the pack meets the performance requirements of the application. However, due to the inherent degradation mechanisms and inconsistencies in operating conditions for cells within a series connected battery pack, there is a differential in the State-of-Health (SoH) of cells which subsequently affects the utilizable energy of the overall pack. Thus, it is imperative to have models which rely on short duration tests to rapidly estimate the SoH of the battery packs. In this project, two of the most widely used Li ion battery types – Nickel-Manganese-Cobalt (NMC) and Lithium-Iron-Phosphate (LFP) chemistry cells are evaluated.

An empirical model is proposed which relies on two quick 10 second pulses to estimate the SoH of a battery pack consisting of 4 series connected cells. The empirical models are trained with a variety of series connected battery packs constructed using combinations of differently aged cells. The model yields excellent results for the NMC chemistry battery packs with Root-Mean-Squared Error (RMSE) of 2.05 Total SoH % points and Mean Absolute Error (MAE) of 1.60 Total SoH % points. However, the LFP chemistry of cells only achieve an RMSE of 6.09 Total SoH % points and MAE of 4.81 Total SoH % points. The hypothesis is that this performance differential exists due to the much steeper Open Circuit Voltage – State of Charge (OCV-SoC) curve for NMC cells over LFP cells. Further tests expanding the range of SoH of packs is recommended along with additional models to also estimate information about the distribution of SoH of the constituent cells are suggested as part of future work.

Acknowledgements

I would like to take this opportunity to express my deepest gratitude towards Dr. Jae Wan Park in providing his patient guidance, enthusiastic encouragement and continued support towards the completion of this project and continuation of this particular research arena.

I would also like to express utmost appreciation of my lab partner and dear friend Lucas Beslow in being an integral part of this project work, without whom this project would not have been completed and taken forward.

I would also like to express my gratitude to Dr. Joseph Lacap who was instrumental in helping me understand and safely operate the various test equipment in our laboratory, along with in depth explanations on the physics of Li ion batteries.

I also would like to express my gratitude to Dr. Alan T Jenn for his guidance and direction in the crucial statistical analysis portion of our project and the valuable time from his schedule which he has taken out for us.

Finally, I would also like to thank Distinguished Professor Dr. Bryan M Jenkins for being a part of my committee and providing his time, patience, encouragement and valuable feedback in the completion of my thesis.

.

Contents

Chapter 1: Introduction

1.1 Background

Electric Vehicles are one of the most promising solutions in the transportation sector for addressing climate change. After the energy spent in production of EVs, the greenhouse gas emissions almost exclusively depend only on the energy source for charging the vehicles. Lithium-ion batteries form the heart of any battery-electric vehicle as they are the energy stores which replace the role of fuel in Internal Combustion Engine vehicles. In addition to being energy stores for electric vehicles, Lithium-ion batteries can also be used for energy storage in electric grids. This presents an opportunity to use electric vehicle batteries for a second life purpose as part of a stationary Energy Storage System (ESS) for commercial or residential use at the end of life (EOL) of the EV batteries. It is commonly considered that a battery reaches its EOL when its capacity is around 80% of its rated capacity [1]. However, one of the main concerns in such applications is that the Li-ion cells used in EVs are almost always connected in a combination of series-parallel connections to provide the appropriate current and voltage from the battery pack. This is usually different from the requirements of an ESS for both commercial and residential applications. This project in particular focuses on the series connected parts of the modules which make up the battery storage in the EVs. As will be described in section 1.2 ahead, the degradation of Li ion cells connected in series is not always uniform, which leads to a significant loss of capacity of that module. This is because the module capacity, in operation, is limited by the capacity of the cell with the most degradation within a module/pack. To address this issue, it is important to be able to estimate the theoretical maximum capacity of a module to determine if there is a significant difference in the capacities of the cells which constitute a series connected battery module/pack. This has two important potential applications; namely this will enable in deciding how the battery reconnections are to be made in

order to ensure that the ESS has the maximum energy storage capacity possible during its operation. Secondly, it can be used as part of a diagnostics procedure during the maintenance and operation of EVs as well.

In the following sections, the basic Li ion battery degradation mechanisms are described in brief, followed by different cell modeling techniques. Next, the State-of-Health (SoH) estimation methods at a single cell level are presented. There are many studies available in literature with effective and accurate models for estimating the SoH of a single cell. However, there are additional factors affecting the estimation of SoH when a number of cells are connected in series to form a battery pack. These factors are explored by taking a look at inconsistencies that arise in the battery pack, followed by practical cell balancing methods applied in EVs to address these. Finally, SoH estimation studies aimed at series packs are presented, and the gap in research that this project aims to fill is emphasized, which will conclude this chapter.

1.2 Literature Review

As the various studies on degradation mechanisms and modeling of the SoH estimation are presented later in the chapter, there are a few Li ion battery nomenclature terms that are establish first:

1. Nominal Capacity (Qn), defined as the maximum usable charge stored in a battery. It is measured in Ah, where the battery has the capacity to yield 1A of current for 1 hour.
2. State-of-Charge (SoC in %), defined as the ratio of the available capacity Q(t) and the maximum possible charge that can be stored in a battery, i.e., the nominal capacity Qn.

$$SoC(t) = \frac{Q(t)}{Qn} \times 100\%$$

3. C-rate is a measure of the rate at which a battery is charged/discharged relative to its maximum capacity. For instance, a 1C rate means that the discharge current will discharge the entire battery in 1 hour.
4. State-of-Health (SoH in %): Formally, there are two definitions of State-of-Health of a Li ion battery. They are:

   (i) By capacity: The ratio of the current capacity of the cell to the rated capacity or the nominal capacity of the cell. It is given by:

$$SoH = \frac{Q}{Qr} \times 100\%$$

   Where Q - current capacity of cell

   Qr - rated/nominal capacity of cell

   (ii) By internal resistance: The ratio of the difference in the internal resistance of a cell at end of life and present state, to the difference in the internal resistance of a cell at end of life and when the cell is new. It is given by:

$$SoH = \frac{Re - R}{Re - Rn} \times 100\%$$

Where Re - internal resistance of battery at end of life

R - present internal resistance of battery

Rn - internal resistance of a new battery

Note that the effect of this definition is seen in the power capability of the battery. As the internal resistance increases with aging there is an observable power fade. [2]

5. Cutoff Voltages (V): The charge and discharge cutoff voltages are those at which the battery is considered fully charged or discharged, and a further charge or discharge of the battery would be considered unsafe.
6. Coulombic Efficiency (η) refers to the ratio of the discharge capacity after the full charge and the charging capacity of the same cycle. It is usually a fraction of less than 1.
7. Open Circuit Voltage (OCV in V), the voltage measured across the positive and negative terminals of a battery, after it has rested for a considerable period. The OCV is a function of the State-of-Charge (SoC) of a cell and is monotonously increasing with the SoC for all cell chemistries.

1.2.1 Li ion Battery Degradation Mechanisms

Lithium-ion batteries age due to various physical and electrochemical reactions which take place both during their operation as well as when they are at rest. The nature and rate of the degradation depends on the particular cycling conditions, but the overall trend when it comes to capacity fade of lithium-ion batteries stays the same. In general, most of the degradation mechanisms are common across various Li ion cell chemistries with only a few exceptions. Therefore, the general degradation mechanisms are described here. This is depicted in fig. 1, which consists of the initial acceleration stage, followed by the stabilization phase, which is mostly linear, and finally the saturation stage where there is a relatively expedited loss of capacity.

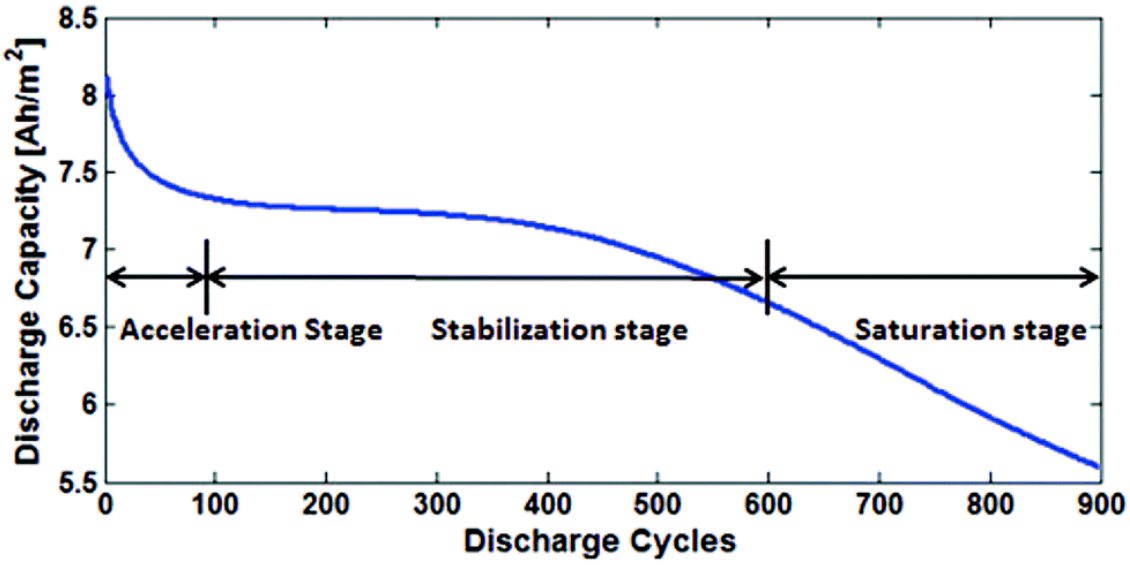

Figure 1: Typical degradation of Li ion batteries over usage [3]

For the purpose of this project, the first definition of SoH is considered, involving cell capacity to denote State-of-Health (SoH) of a battery. Next, the major degradation modes and associated mechanisms involved are looked at. The following figure (fig. 2) provides a schematic representation of the various degradation mechanisms.

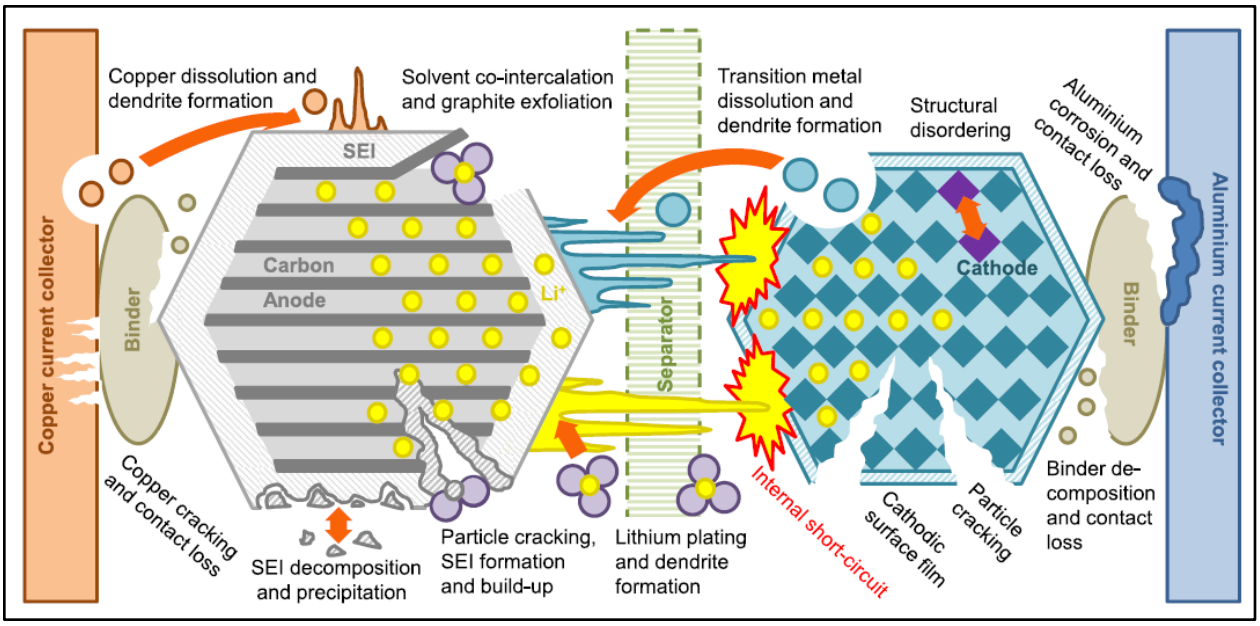

Figure 2: Degradation mechanisms in Li-ion cells [4]

The main degradation modes are described here, followed by the mechanisms involved [4]:

1. Loss of Lithium Inventory (LLI): In this degradation mode, there is a loss of active Li which can participate in the charging and discharging of the cell. This could be due to surface film formation (SEI layer), lithium plating, island formation, which are described later.
2. Loss of Active Material (LAM): This can occur at both the anode and cathode of a cell. At the anode side, this involves the loss of active mass of the anode as there is a reduction in the availability of sites for the insertion of lithium ions. This could be due to particle cracking or loss of electrical contact due to resistive layers. At the cathode side this implies that there is a loss of active mass of cathode material where lithium can be inserted during the discharge. This could be due to structural disordering, particle cracking or due to loss of electrical contact.
3. Reduced Kinetics: This involves slowing of the insertion and exit of the lithium ions from both the anode and cathode sides of the cell. This can be due to increased tortuosity,

transition metal dissolution or misalignment in the cathode structure. It affects the reaction rates during both charging and discharging of the cell.

4. Increased Electrical Resistance: In this degradation mode, there is an increase in the electrical resistance of the cell which can be caused by growth of the SEI layer, dissolution of current collectors and enhanced surface film formation around the particle cracking sites.

The degradation mechanisms which are responsible for the aforementioned degradation modes are briefly discussed as follows:

1. The Solid Electrolyte Interphase (SEI Layer) is what forms when the electrolyte comes into contact with the anode material. Initially the rate of SEI formation is rapid and once a sufficiently thick SEI layer is formed, the rate of growth slows down and stabilizes. This phase of rapid SEI formation is what corresponds to the acceleration stage depicted in fig. 1. As a result of the SEI growth, there is an increase in the electrical resistance of the cell. Note that the temperature plays an important role in the rate of growth of the SEI layer, which is accelerated at elevated temperatures. Furthermore, this mechanism continues to occur at a slow rate even when the battery is at rest. This is the cause of the phenomenon of 'calendar aging', whereby the capacity of a cell decreases even when at rest.
2. Lithium plating occurs at each, or a combination of - high State-of-Charge (SoC - meaning battery close to 100%), high charge rate and low temperatures. When the Li ions are traveling from the cathode to the anode, if there is not sufficiently quick diffusion of Li into the anode, all of the Li may not be able to de-solvate from the electrolyte, resulting in the Li ions preferentially bonding with the Li metal instead of diffusing into the anode. This can lead to damage of the layered graphite structure and more crucially, lead to dendrite formation of the metallic lithium, which if happens over an extended period of

time could lead to short circuit of the cell if the Li dendrites reach across the electrolyte over to the cathode side. It also leads to a loss of lithium inventory (LLI) as this lithium is no longer available for participation in the charging and discharging process.

3. Microcracks and island formation occur due to mechanical stresses imposed on the anode and cathode sides during full charge and discharge cycles, especially at high currents. In some chemistries, this can lead to a volume change of up to 13% at the anode over a complete cycle. The mechanical stresses involved can lead to some portions of the cathode to undergo structural misalignment resulting in increased tortuosity and therefore, reduced kinetics. Furthermore, there can be island formation at the anode, whereby pockets of the graphite structure get electrically insulated due to structural breakage. This can simultaneously cause LLI and LAM, since the lithium also gets trapped in the anode pocket/island. This can also lead to further SEI formation around the anode which increases the electrical resistance of the cell.
4. Loss of electrical contact can occur at very low State-of-Charge (SoC) whereby the anode and/or cathode current collectors may dissolve due to their potentials falling outside of the electrochemical stability window. This can directly lead to increase in electrical resistance and aluminum/copper dendrite formation which can also potentially lead to microcracks themselves along with its associated effects.
5. Transition metal dissolution can occur at high temperatures and SoC, causing dendrite formation at the cathode side (especially with Mn as a cathode material), leading to similar safety concerns as lithium plating. This also leads to a loss in the number of sites for the lithium to form the metal oxide at the cathode, and hence to LAM. Furthermore, at high

currents the cathode may undergo misalignment in its structure, reducing its diffusivity and therefore, a reduction in kinetics slowing down the charge and discharge.

A summary of the operating conditions, associated degradation mechanisms and modes, and their corresponding effects is provided in fig. 3 as follows:

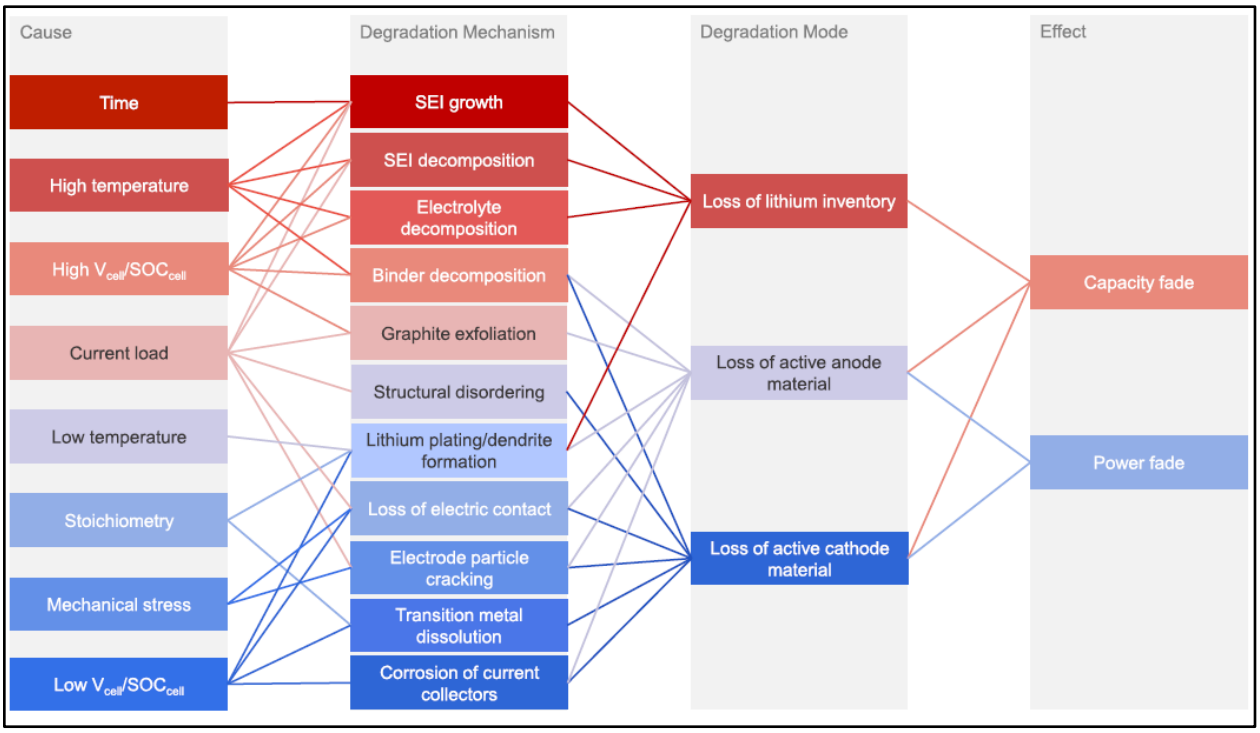

Figure 3: Cause and effect of degradation mechanisms and associated degradation modes [4]

1.2.2 Modeling the Degradation Mechanisms

As described in the previous section, there are various physical and electrochemical mechanisms involved in the degradation of Li ion cells. This makes the modeling of these mechanisms extremely challenging. A true electrochemical model is considered to have high mathematical complexity, and therefore a more popular model used instead is the Pseudo-2D (P2D) electrochemical model which simplifies the model with many assumptions. The key equations in such a model are presented below:

Electrochemical model framework		Boundary Conditions
Electrolyte phase $i = N, S, P$		
$\varepsilon_{ey,i}F\frac{\partial c}{\partial t}+\frac{\partial J_{conc}}{\partial x}=(1-t_+)J^V_{ct,i}$	(1)	$J_{conc}\vert_{x=1}=0;$ $J_{conc}\vert_{x=4}=0$
$J_{conc}=-\frac{\varepsilon_{ey,i}}{\tau_{ey,i}}F\tilde{D}\frac{\partial c}{\partial x}$	(2)	
$\frac{\partial J_2}{\partial x}=J^V_{ct,i}$	(3)	$J_2\vert_{x=1}=0;$ $J_2\vert_{x=4}=0$
$J_2=-\frac{\varepsilon_{ey,i}}{\tau_{ey,i}}\sigma\frac{\partial\tilde{\mu}^*_+}{\partial x}+\frac{\varepsilon_{ey,i}}{\tau_{ey,i}}\sigma\frac{2RT}{F}(1-t_+)\gamma_\pm\frac{\partial \ln c}{\partial x}$	(4)	
Active material phase $i = N, P$		
$F\frac{\partial c_{s,i}}{\partial t}+\frac{\partial J_{s,i}}{\partial y}=-\frac{2}{y}J_{s,i}$	(5)	$J_{s,i}\vert_{y=0}=0;$ $J_{s,i}\vert_{y=r_{s,i}}=J_{ct,i}$
$J_{s,i}=-FD_{si}\frac{\partial c_{s,i}}{\partial y}$	(6)	
Charge balance equations $i = N, P$		
$\frac{\partial J_{1,i}}{\partial x}=-J^V_{ct,i}$	(7)	$\tilde{\mu}^*_{e,N}\vert_{x=1}=0;$ $J_{1,N}\vert_{x=2}=0$ $J_{1,P}\vert_{x=3}=0;$ $J_{1,P}\vert_{x=4}=\pm I_{app}$
$J_{1,i}=-\frac{\varepsilon_{el,i}}{\tau_{el,i}}\sigma_{e,i}\frac{\partial\tilde{\mu}^*_{e,i}}{\partial x}$	(8)	
$J^V_{ct,i}=J_{ct,i}A_{am,i}$	(9)	
$J_{ct,i}=i_{00i}c^\alpha(c^{\max}_{s,i}-c_{s,i})^\alpha c^{1-\alpha}_{s,i}\left[\exp\left(\frac{\alpha F}{RT}\eta_{act,i}\right)-\exp\left(-\frac{(1-\alpha)F}{RT}\eta_{act,i}\right)\right]$	(10)	
$\eta_{act,i}=\tilde{\mu}^*_{e,i}-\tilde{\mu}^*_{+,i}-U_{eq,i}$	(11)	

Figure 4: Equations of the electrochemical P2D model. [5]

For a comprehensive description of the equations and nomenclature, please refer to the study by [5]. From this electrochemical model the 6 main parameters are considered in 3 groups as follows:

1. Solid State Diffusivities (D_{sn} and D_{sp}): A reduction in diffusivity indicates an increase in microcracks, along with possible misalignment of the cathode material leading to increased tortuosity.
2. Ambipolar diffusivity (D) and conductivity of electrolyte (σ): SEI formation and subsequent growth along with decomposition of electrolyte leads to a decrease in the electrical conductivity of electrolyte.
3. Kinetic constants of intercalation reactions (i_{00n} and i_{00p}): The growth of SEI layer into and around the island formation regions in the anode, along with the detachment of carbon-binder-domain leads to a reduction in the active surface area of the anode.

These 6 main parameters described above can also be modeled using an equivalent electrical circuit. Hence, it is called an Equivalent Circuit Model (ECM) and is a highly popular model in literature due to its simple formulation, low computational effort and an easy physical and electrochemical interpretation. A brief description of this type of modeling is described in the figure below:

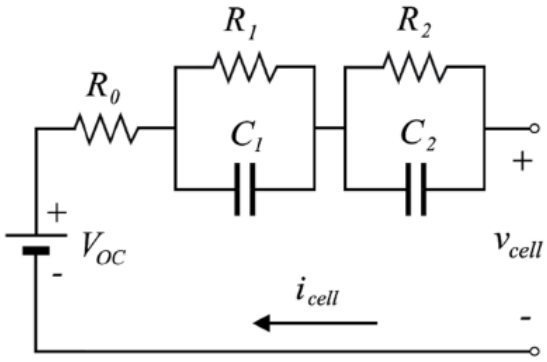

Figure 5: ECM representation using 2RC pairs [6]

In this type of model, the series resistance R_0 represents the instantaneous response, while the RC pairs represent the time varying dynamic response. As the number of RC pairs are increased, the computational complexity increases substantially, but the model accuracy does not increase considerably beyond 2 RC pairs [7]. Hence, the 2RC model is considered an optimal tradeoff between model accuracy and computational load. The interpretation of each of the parameters is given below [6]:

1. R_0 represents Very Fast Dynamics (VFD), time scale <4s
2. First RC pair includes Fast Dynamics (FD) and part of Slow Dynamics (SD) with time scales of 4s to 5 mins
3. Second RC pair includes Slow Dynamics (SD) and some of Fast Dynamics (FD) with time scales of 3 mins to 100 mins

The correlation between the physical/electrochemical parameters and the ECM parameters is as follows [6]:

1. Variation of R_1 and C_1 is exclusively linked to electrolyte parameters, indicating SEI growth or electrolyte decomposition.
2. Variation of R_2 and C_2 is exclusively linked with the solid state diffusivities, which could be the result of microcracking causing increased tortuosity.
3. R_0 increase is linked to the changes in the kinetic constants, caused by SEI growth into the anode, detachment of carbon binder diminishing the active area of the electrode.

With these correlations and their interpretations in mind, the SoH estimation methods for a single cell are discussed in the following section.

1.2.3 SoH estimation methods at a Single Cell Level

The various SoH estimation methods at a single cell level can broadly be classified into Physics Based Methods, Empirical Models, Incremental Capacity Analysis (ICA) based methods and Data-Driven Approach methods. Their brief descriptions, key benefits and drawbacks are summarized in the following figure:

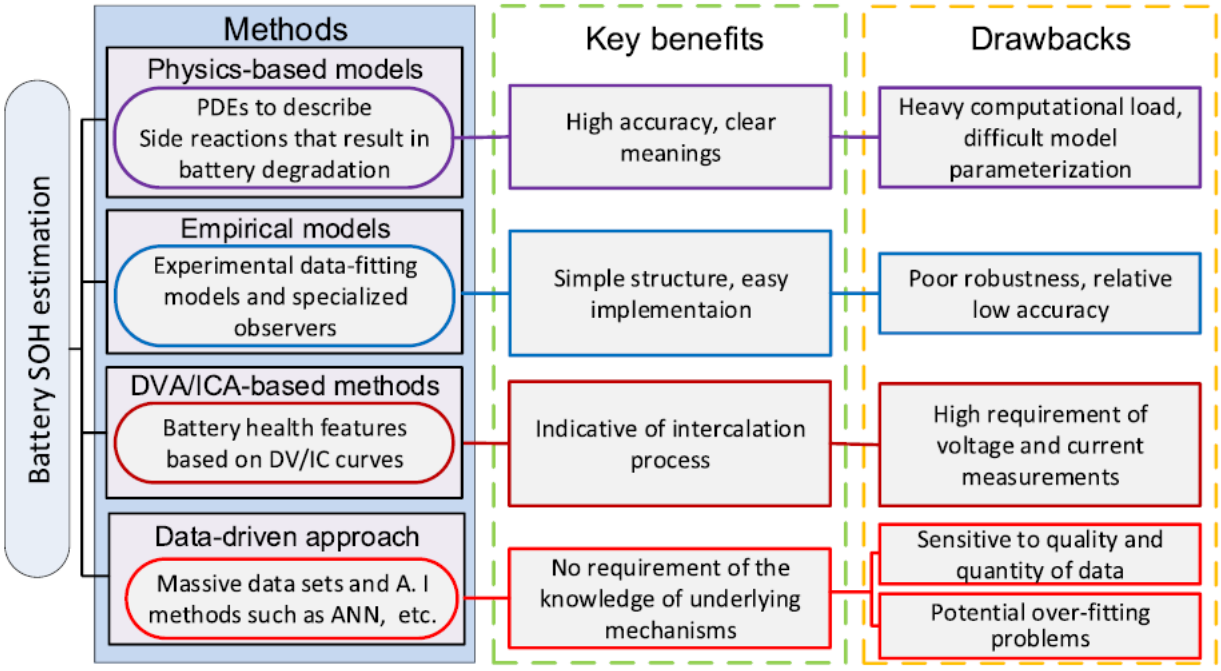

Figure 6: Battery SoH estimation methods, key benefits and drawbacks [8]

A brief overview is provided here as follows:

While the physics-based methods provide the best physical and electrochemical information and interpretation, the excessively high computational load along with difficulty in obtaining the accurate parameter values through experimentation results is a considerable drawback.

Empirical models derived based on fitting experimental data on the other hand have the least computational load. However, the correlation between the obtained parameters and the

physical and electrochemical properties is quite unclear, leading to lower accuracy if a battery with substantially different electrochemical parameters is to be estimated for. An example of such a model is the investigation by [9]. This empirical study made use of nonlinearity of internal resistance dynamics with aging to create empirical models that could predict the SoH of cells based on the data from as little as 5 initial cycles of the cell. For reference, here are the internal resistance vs battery capacity graphs for the same current but different operating temperatures along with the model parameters.

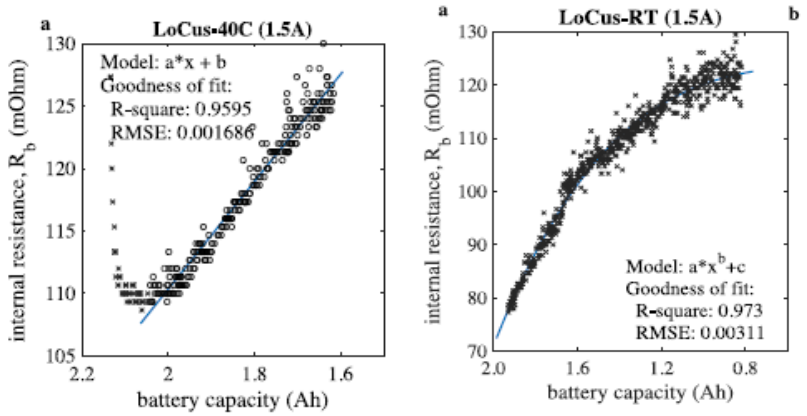

Figure 7: Empirical SoH model based on internal resistance at different temperatures [9]

Incremental Capacity Analysis (ICA) methods are more recent and proving to be quite effective in predicting the SoH of cells based on the charge capacity held in different voltage segments of a cell. The charge capacity held within a particular voltage range in this case is also referred to as a Health Indicator (HI). As the cell ages, the charge capacity that it can hold at a given voltage range changes. This is illustrated in fig. 8.

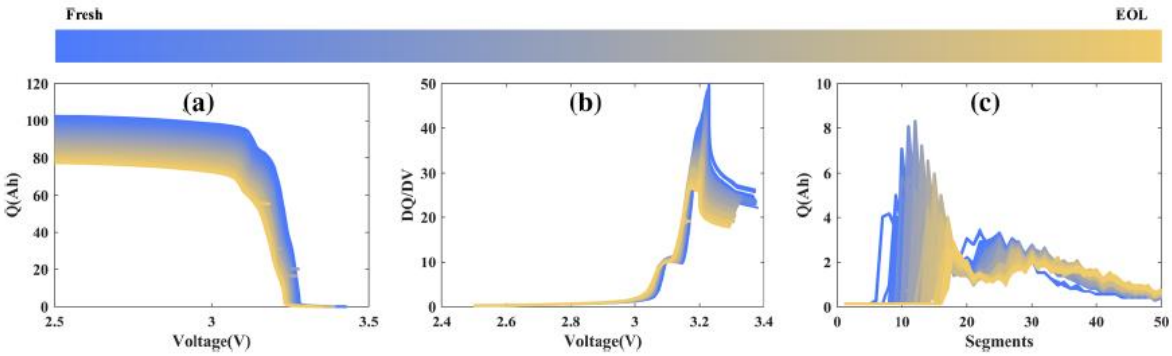

Figure 8: a) Q-V curve of a cell over lifetime, b) Incremental Capacity (IC) curve over lifetime, c) ΔQ sequence curves of cell over lifetime [10]

Based on the section(s) which have the highest correlation between the DQ/DV and the SoH of a cell, the ICA based model is created. For a more in-depth explanation and analysis, the reader is referred to [10].

Data-driven approaches like Artificial Intelligence and Neural Networks, are quite effective in predicting the SoH, if there is a large quantity of data available. Generally, these tests involve testing the batteries under certain conditions which provide the greatest correlation between the SoH and the particular parameters being measured. Potential drawbacks are over-fitting to a certain type of cells/cycling conditions and lack of correlation between the model structure and the physical and electrochemical properties. There are several studies that involve using AI and the reader is encouraged to follow [8] for further reading.

In terms of estimating the SoH for a single cell, there are plenty of models available in literature which are robust, accurate and reliable. However, when it comes to estimation at a pack level, there are additional factors that come into play. These are discussed in the following section.

1.2.4 Inconsistencies in Series Packs and Cell Balancing

Inconsistencies in the context of series connected battery packs refers to the variation in critical parameters of batteries within a pack. These are namely:

1. Capacities of the cells
2. Internal resistances of the cells
3. States-of Charge (SoC) of each of the cells
4. Coulombic Efficiency of each of the cells - refers to the ratio of the discharge capacity after the full charge and the charging capacity of the same cycle.

When the battery packs are operated with such inconsistencies, the magnitude of these inconsistencies tends to increase over time. Now, there are two primary reasons for inconsistencies in parameters in battery packs [11]:

1. Inconsistencies at Production Stage - Since no production technology is perfect, there are always minor variations in the parameters of the batteries as they are produced and connected together to form a battery pack.
2. Usage Conditions - The C-rates, SoC range of operation, thermal distribution within a pack are some of the usage conditions which can exacerbate the inconsistencies.

As an example, to illustrate these inconsistencies, fig. 9 shows the parameter distribution of a battery pack with 95 cells taken from[12].

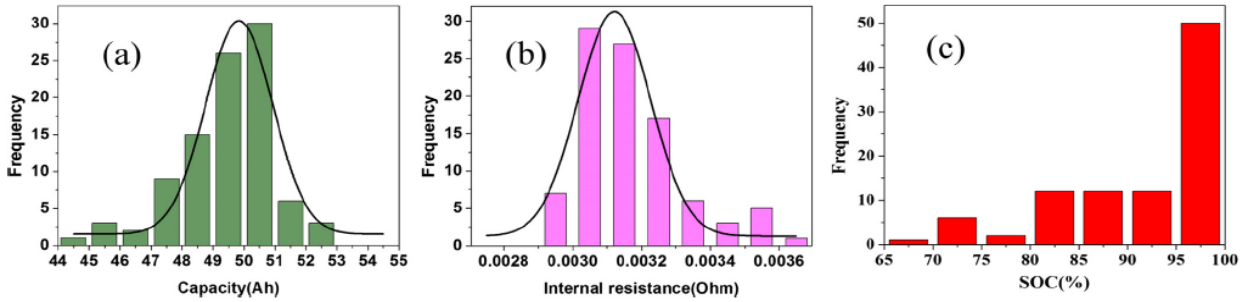

Figure 9: Parameter distribution of a battery pack with 95 cells [12]

Among these four parameters, it was found through sensitivity analysis by[11], that the total capacity, i.e. the utilizable energy of a series connected battery pack is lowered the most when there is a variation in the SoC of the cells constituting a pack. Therefore, in practical operation of battery packs it is crucial to minimize the SoC variation. Furthermore, it was also found that SoC variation is exacerbated the most when the coulombic efficiency of the cells within a pack is different.

In order to address the issue of SoC variation, a commonly applied technique during operation is that of Cell Balancing. Balancing or Equalizing is the process of modifying the level of charge in cells on a cell-by-cell basis. A balanced battery pack is one in which at some point in its cycle, all the cells are at exactly the same SoC. There are two basic approaches to equalizing:

1. Passive balancing - drains from higher SoC cells and dissipates as heat
2. Active balancing - moves charge from “high cells” to “low cells” attempting to conserve charge

Nearly all balancing concepts require Battery Management System (BMS) control of balancing activities. A schematic diagram to explain the concept of balancing is shown in fig. 10.

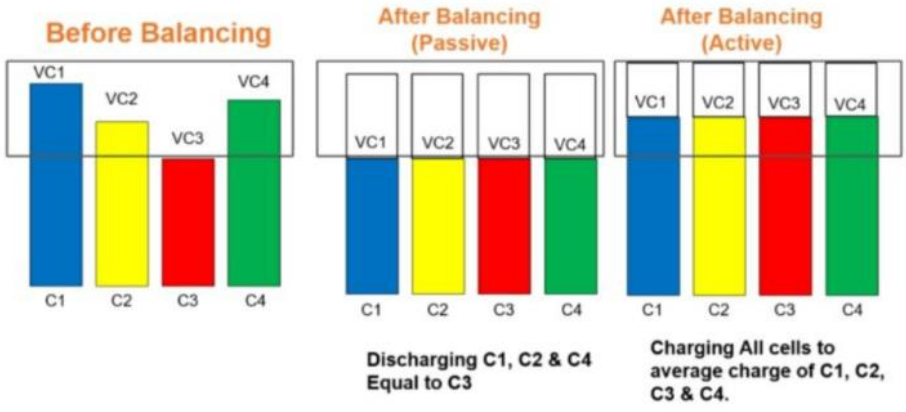

Figure 10: Schematic diagram of active and passive cell balancing[13]

A classification of different cell balancing techniques is shown below, taken from [13].

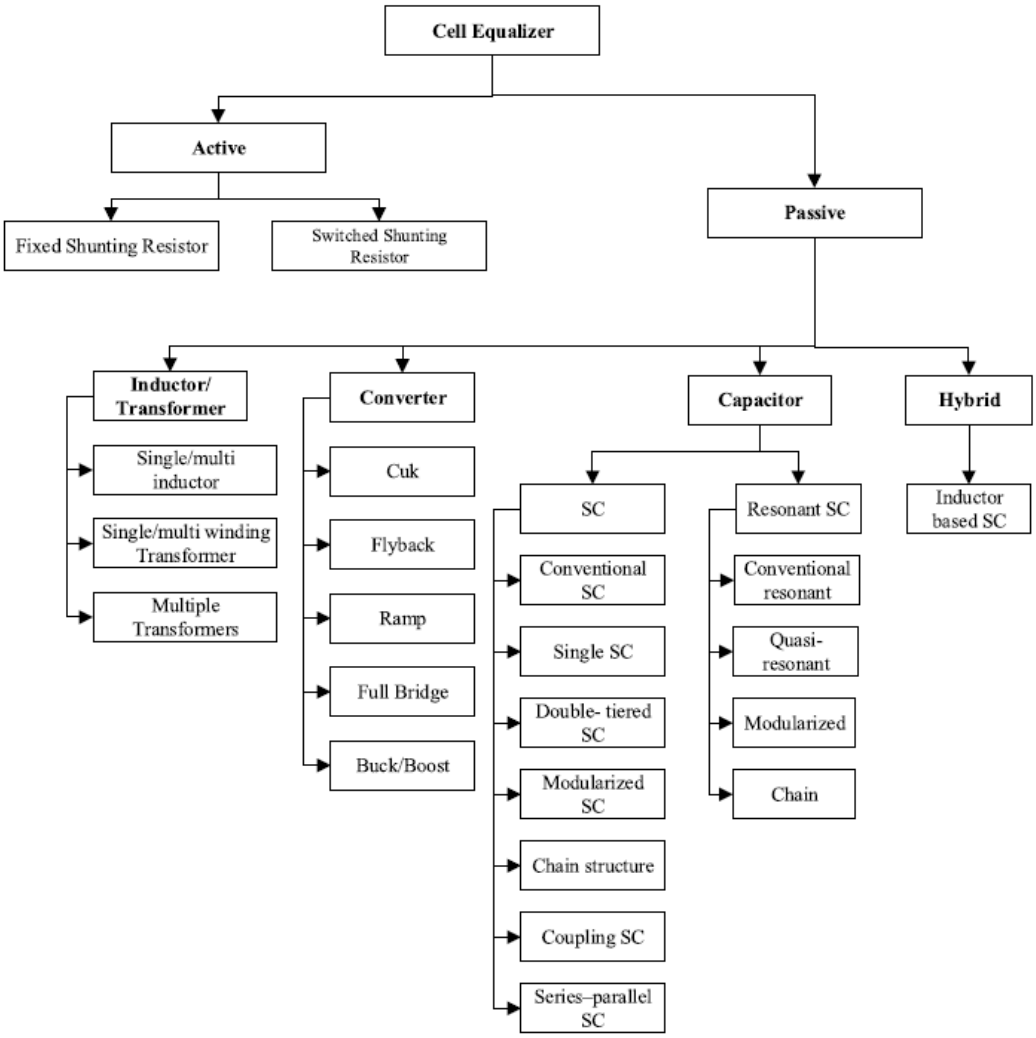

Figure 11: Classification of Cell Balancing Techniques [13]

For further information regarding the individual balancing techniques, the reader is directed to [13] which provides a comprehensive review. In addition to the types of balancing techniques, there are three primary considerations to be made when applying the balancing techniques:

1. Set point: The SoC at which the cells should be balanced, i.e. 0%/50%/100%, alternatively they can be balanced dynamically with fast active balancing
2. Measurement Parameter: Balancing can based on either SoC estimates, Voltage measurements, or on total energy available in a pack

3. When to Balance: Balancing can be done while charging only, or on a continuous basis or on a predictive basis.

All these considerations go hand in hand when deciding the particular balancing technique that is to be employed. In general, it can be said that active balancing ensures minimal energy loss from the battery packs and also ensures a more uniform degradation rate within a pack. Note that some techniques are better suited for EV applications, while others may be better suited for ESS applications. The most important point to note here is that most EVs employ passive balancing techniques as it is far more cost effective as compared to any other active balancing method. Thus, it is found that over time, there is almost certainly a divergence of cell parameters, especially cell capacity which further enhances the need for estimation of SoH of a battery pack. In the next section, the State-of-Health of a battery pack is formally defined, and the broad range of studies conducted in SoH estimation for packs are discussed in brief.

1.2.5 SoH Estimation of a Battery Pack

There are two ways to define the State-of-Health (SoH) of a battery pack:

1. Based on the current available energy - with cell-to-cell variation

$$SoH_{dif} = \frac{Present\ Available\ Energy}{Initial\ Maximum\ Available\ Energy} \times 100\%$$

   In this definition, the present available energy is determined by the cell with the lowest individual SoH. The present available energy would be the energy obtained from the pack when discharging it divided by the original maximum capacity: as soon as the lowest SoH cell reaches the discharge cutoff voltage, the cumulative capacity till that point would constitute the present available energy, even if there are other cells within the same pack which can still discharge further and yield more energy.

2. Based on the theoretical maximum available energy - without cell-to-cell variation

$$SoH_{max} = \frac{Present\ Maximum\ Available\ Energy}{Initial\ Maximum\ Available\ Energy} \times 100\%$$

   By this definition, the total SoH of a pack would simply be the sum of the capacities of the individual cells divided by the original maximum capacity, regardless of whether each cell can practically provide a full discharge whilst still in the pack.

Since the second definition is the relevant one from the point of view of 2nd life ESS application, this definition is adopted for the remainder of the thesis with a slight modification as explained in section 2.2. When it comes to the estimation of SoH of battery packs, the majority of estimation methods can again be categorized as in fig. 6. A broad view of the literature on estimating the pack SoH is presented by looking at a few prominent studies.

Bi et al. [14] investigated the use case of electric taxis in Beijing whereby they proposed modeling the entire series connected battery pack as a single 2nd order ECM model and developed

a genetic resampling particle filter (GPF) model based on it. This approach greatly reduced computational burden as opposed to modeling every single cell but it is stated that further verification was required for greater cell-to-cell SoH variation.

Numerous studies such as by Hua et al.[15], Cordoba-arenas et al.[16] and Diao et al. [17] estimated the pack SoH by modeling each cell using either a 1st order or 2nd order ECM model. Some of the mentioned studies also incorporated estimation of SoC into their models as well, yielding accuracy as high as 3% Mean Absolute Error (MAE). Yu et al. [18] proposed creating an electrochemical model for each cell of a series pack consisting of 6 cells in series. The cells would first undergo capacity checks followed by pulse tests to determine the electrochemical parameters which yields information on SoC and SoH with MAE being around 2.2%.

Multiple studies also took the approach of Incremental Capacity Analysis (ICA) and combining it with Machine Learning models. Che et al. [10] made use of Transferred Deep Learning (TDL) and Gaussian Process Regression (GPR) to predict the SoH of individual cells and then the subsequent pack SoH. The data being fed to the model was of the IC curves of each cell between 3.15-3.3V during the discharge of cells. At pack level this implied MAE and RMSE of around 3.5%. Yonghuan et al. [19] applied ICA to differently aged LFP chemistry cells and established the correlation between the positions and magnitudes of the peaks on the IC curves, with the capacities of the cells. This yielded an estimation error of within 1% for the State of Disequilibrium (SoD), which is the maximum difference in the capacities of cells within a pack of 8 series connected cells.

Some studies such as by Song et al. [20] and Huotari et al. [21] take a big data platform approach whereby [20] analyzed data from 700 cars while [21] from 45 forklifts over varying periods of time. The data analyzed consisted of accumulated mileage - proxy for number of cycles,

C-rates and charging times, ambient temperature during operation and intensity of SoC ranges. [20] yield results as good as 4.5% maximum SoH estimation error, while [21] an MAE of 0.29 SoH was obtained.

Whilst the aforementioned studies also largely fit into the categorization of SoH estimation methods proposed in figure 6, there are some exceptions whereby a different approach is taken. For example, Love et al. [22] proposed an impedance measurement method for monitoring the SoH of individual cells in a pack consisting of 4 cells connected in series. It was found that the overcharge abuse could be detected through the statistical $\mu \pm 3\sigma$ standard deviation threshold in the impedance response. Song et al. [23] conducted a study on a pack of 9 series connected LCO chemistry cells and analyzed them over 5000 cycles. It was found that as the cells aged the charge cutoff voltage of the overall pack reduced over time. This reduction is the result of increase in the inconsistency within the pack over time, which can be a proxy for the SoH degradation. They reported a Spearman's rank correlation coefficient of -0.88 and suggested that both the inconsistency and pack SoH could be monitored. Xu et al. [24] employed a signal processing technique called Discrete Wavelet Transform (DWT) which is used for micro resolution analysis (MRA). This was used to analyze the voltage measurements of each of 5 NMC chemistry cells connected in series over a number of drive cycles run on them. Note that the features identified with this method are independent of the SoC of the cells involved, which is not the case for most of the studies mentioned previously. This technique yielded a maximum pack SoH estimation error of 1%.

The studies discussed above broadly cover nearly all categories of research in the current state of SoH estimation. The reader is encouraged to follow reference [25] as well as other review papers published in this domain for further reading.

1.3 Research Gaps and Proposed Solution

The following points provide a concise summary of the literature review presented in 1.2:

1. There are a multitude of degradation mechanisms arising from different operating conditions of Li ion batteries, regardless of their chemistry. These mechanisms cause different effects on the 4 primary degradation modes of LLI, LAM, Reduced Kinetics and Increased Electrical resistance. All these modes combined contribute to the capacity fade resulting in the degradation of the SoH of a battery.
2. Modeling these effects is achieved most widely by employing the Equivalent Circuit Model (ECM) which are computationally simple, and the effects of the resistances and capacitances can be correlated with the physics and electrochemistry of the processes within a cell.
3. There are 4 broad categories of estimation of SoH of a single cell, which include electrochemical models, empirical models, ICA based models and Machine Learning models. These methods have been researched extensively and the right models based on the application can provide excellent results.
4. However, when moving from a single cell level to pack level, then the phenomenon of inconsistency in parameters among the cells arises. This refers to the fact that the cells connected in series have 4 parameters which are different from one another; namely the SoC, SoH, Coulombic efficiency and internal resistance. If left unchecked, these parameters keep diverging as the pack is operated over time, leading to further nonuniform degradation of the cells along with reduced energy available from packs. Cell balancing is widely used in EVs and in ESS to mitigate these inconsistencies. This involves making a choice between passive and active balancing of the cells, and due to the higher complexity and costs associated with active balancing, most EVs are equipped with passive balancing

systems. This further contributes to divergence of parameters, especially the SoH of the cells within a pack.

5. Hence it is imperative to have models to estimate the SoH of battery packs accurately for both diagnostics as well as for repurposing them for 2nd life ESS use. Broadly these models can be classified on a similar basis as the single cell SoH estimation models, with added complexities due to the additional cells.

However, the following gaps in the literature are identified, which this study aims to address:

1. Most models in literature make use of the recorded cell voltages from each of the cells, except for very few studies such as [21] which only record the overall pack voltages and not the individual cell voltages. In practical BMS applications in EVs, the voltage of each cell is measured but not committed to memory as there could be hundreds of cells in the vehicle [20]. The instantaneous measurements are only for ensuring the safe voltage operation of the pack and the measurements are discarded immediately once they are made.
2. On one hand the Machine Learning models require collection of a large amount of past operational data, while many of the other types require conducting relatively long discharge pulses such as the ICA based models. While the 2nd order ECM models can be constructed with smaller tests which include simple pulse tests, these again require measurement of the cell voltage of each individual cell over the entire pulse duration.

Therefore, based on the above two prominent gaps in literature, the following method to estimate the SoH of a given battery pack is proposed, which most importantly includes:

(i) A short duration, simple pulse test which neither requires vast amounts of past operational data, nor running a given pack for several minutes to even hours such as in ICA based methods.

(ii) Voltage measurement only at the pack level, which is what is practically employed in Battery Management Systems (BMS) in EVs.

A pulse test was selected as it was shown in multiple studies which proposed ECM models that extraction of the R_0, R_1-C_1 and R_2-C_2 parameters was effective using pulse tests and that the tests themselves were brief. As these parameters also varied with the progressive degradation of cells, they could be a proxy for cell SoH, and when connected in series, their added effect could be captured by the voltage response of the overall pack.

The only drawback of the proposed methodology is that all the cells are required to be brought to a balancing point of 50% SoC. However, it is to be noted that this is also a common practice in EV and residential BMS to be selecting 50% SoC as the balancing point. The rationale for selecting 50% SoC as the balancing point was that both the charge and discharge pulses could be of a high current magnitude, without the cells hitting the upper or lower voltage cutoffs as the current was being passed. Neither higher nor lower SoC balancing points allowed the possibility of high current magnitudes in both the charge and discharge pulse. Based on the above criteria, a test plan for establishing a SoH model was formulated. The tests were conducted on battery packs consisting of 4 cells in series, on two different widely used Li ion battery chemistries -NMC and LFP, which serves as a proof of concept.

The organization of the remainder of the thesis is as follows: Chapter 2 discusses the experiment methodology and setup, Chapter 3 discusses the setup and results of preliminary tests based on which, Chapter 4 describes the final model, its results and subsequent discussion. Chapter 5 concludes the findings of the project and provides recommendations for future work and Chapter 6 lists the references for further reading.

Chapter 2: Experiment Methodology and Setup

The overview of the experiments is as follows. Firstly, the salient properties of NMC and LFP batteries are presented, followed by the specifications of the cells used in this project. Next, the different combinations of battery packs and their nomenclature used for the experiments are described, along with a brief overview of the tests conducted on the batteries to get them to the desired SoH. Next, the equipment used in the experiments are described along with the final 3D printed fixtures used for holding the batteries. Finally, an elaborate description of the degradation of the batteries and the final set of available batteries and their SoH are presented, which concludes this chapter.

2.1 Properties and Specifications of NMC and LFP Batteries:

In industry, the current market situation is such that the NMC - Nickel-Cobalt-Manganese, and the LFP - Lithium-Iron-Phosphate chemistry of cells are the most widely used [26]. Therefore, it is imperative that these chemistries of cells are to be used for the purpose of this project. The biggest practical difference between these two chemistries of cells is their voltage operation windows. NMC cells are operated between 2.5V - 4.2V whereas LFP cells are operated between 2.5V - 3.65V in most cases. This leads to a difference in the Open Circuit Voltage- State of Charge (OCV-SoC) curves of both the cells. Furthermore, with aging and at different temperatures, there is a deviation in these OCV-SoC curves as depicted in fig. 12 below:

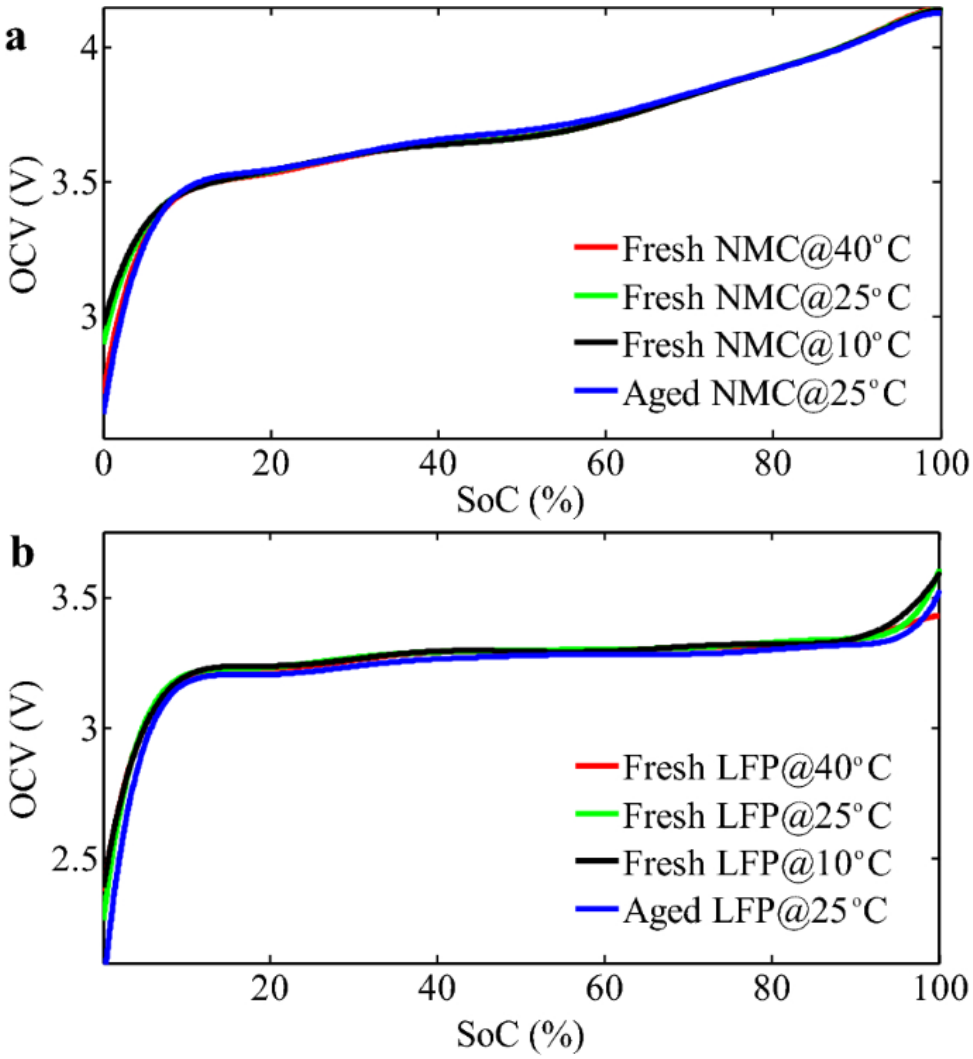

Figure 12: a) OCV-SoC curves for NMC cells, b) OCV-SoC curves for LFP cells[27]

As clear from fig. 12, the OCV-SoC curves are steep for both NMC and LFP cells at low SoC. However, at a significant usage portion for both types, i.e. say between 15%-85% SoC, the curves are largely linear in nature. The NMCs have a slightly steeper slope, compared to the LFP cells which are nearly flat for this entire range. As a ballpark comparison, between 15%-85% SoC, the voltage of the NMC cells changes from ~3.5V to ~3.95V corresponding to an approximate slope of 6.4mV/%SoC, whereas for LFP cells it goes from ~3.2V to ~3.3V corresponding to an approximate slope of 1.4mV/%SoC. For LFPs, there is again a steep incline as the SoC approaches

100%, while much less so for the NMC cells. Next, the specifications of the cells used for experimentation are presented, taken from the manufacturer's datasheets as follows:

Table 1: NMC Cell specifications

Type		**Specification**	**Typical INR18650-25R**
Dimension (mm)	Diameter	18.33 ± 0.07	18.33 ± 0.07
	Height	64.85 ± 0.15	64.85 ± 0.15
Weight (g)		Max. 45.0	43.8
Initial IR (mOhm AC 1kHz)		≤ 18	13.20 ± 2
Initial IR (mOhm DC (10A-1A))		≤ 30	22.15 ± 2
Nominal Voltage (V)		3.6	3.64
Charge Method (100mA cut-off)		CC-CV (4.2± 0.05V)	CC-CV (4.2± 0.05V)
Charge Time	Standard (min), 0.5C	180 min	134 min
	Rapid (min), 4A	60 min	55 min
Charge Current	Standard Current (A)	1.25	1.25
	Max. Current (A)	4	4
Discharge	End Voltage (V)	2.5	2.5
	Max. cont. current (A)	20	20
	Max. momentary pulse (A, <1sec)	100	100
Rated Discharge Capacity	Standard (mAh) (0.2C)	2,500	2,560
	rated (mAh) (10A)	2,450	2,539

Table 2: LFP Cell specifications

Items	**Specifications**
Cell Dimension	Length 65+-0.3mm, Width 18.2+-0.2mm
Charge cut-off voltage	3.65V
Nominal voltage	3.2V
Minimal capacity	1500mAh @ 0.2C Discharge
Nominal capacity	1550mAh @ 0.2C Discharge
Charge current	1C
Standard charging method	1C CC (constant current) charge to 3.65V then CV (constant voltage 3.65V) charge till charge current decline to <= 0.05C
Charging time	Standard charge: 2.0 hours Ref
Max. charge current	2C
Max. continue discharge current	5A (Cell skin temp <80C)
Discharge cut-off voltage	2.0V
Operating temperature	Charging: -10C to 45C Discharging -20C to 60C
Storage temperature/humidity	Temperature -10C to 35C, Humidity 65%+-20%RH
Cell Weight	42.0g+-1.0g

Unfortunately the specifications of the typical LFP cells were not provided by the manufacturer and hence, have been excluded from table 2.

2.2 Battery Pack Definition and Nomenclature

The experiments and analysis were conducted using battery packs consisting of 4 cells connected in series for both the NMC and LFP chemistries. All brand-new cells are prone to inconsistencies resulting from the manufacturing process and hence, do not start off with the exact same State of Health (SoH). In addition to this, the initial formation cycles also see a rapid reduction in capacity due to SEI formation and stabilization, after which the cells exhibit a relatively linear degradation rate [3]. To take these effects and the resulting concerns into account, a brand-new pack with minimal degradation as an "Ideal" pack was defined, which consisted of cells at a uniform State of Health, degraded to 95% SoH each.

In order to denote the total SoH of the pack whilst also expressing granularity of the SoH percentage for convenience, the pack SoH was defined as being the summation of the individual SoH percentages as follows:

$$\textit{Pack State of Health (SoH)} = \frac{\sum_{i=1}^{4} Capacity\ of\ ith\ cell}{Nominal\ Capacity\ of\ a\ Single\ Cell} = \sum_{i=1}^{4} SoH\%\ of\ ith\ cell \quad \textbf{Eq.1}$$

For example, if 4 cells were considered with their SoH being 95%, 90%, 85% and 80% respectively, connected in series, one would denote the pack SoH as being,

$$Pack\ SoH\ or\ Total\ SoH\ = 95 + 90 + 85 + 80\ = 350\%$$

The remaining packs with degraded cells were given a nomenclature code that has the “Ideal” pack as the implicit reference. The pack composition and their corresponding names are listed in the following table:

Table 3: Battery Pack types and their Identifiers

Pack Identifier	# of 95% SoH cells	# of 90% SoH cells	# of 85% SoH cells	# of 80% SoH cells	Proposed Total SoH %
Ideal	4	-	-	-	380%
1C90	3	1	-	-	375%
1C85	3	-	1	-	370%
1C80	3	-	-	1	365%
2C90	2	2	-	-	370%
2C85	2	-	2	-	360%
2C80	2	-	-	2	350%

As shown in the pack identifier column in the table above, the '1C' or the '2C' denoted the number of cells that were replaced from the ideal pack, while the last two digits represented the SoH % of the cells which were replacing the 'ideal' ones. For example, a '1C85' pack implies that one cell from the ideal pack was replaced with a 85% SoH cell. Note that the order of placement (position of cells in the pack) of the cells was not of concern since only the overall pack voltage was considered in the model. The analysis in this project was limited to the above combinations of cells to ensure simplicity in the experimentation and data analysis. However, it is noteworthy that there was still a wide range of variability of the SoH within a pack. The 'Ideal' pack had the most uniform battery SoH while a pack such as a '2C80' pack consisted of cells with highly non-uniform degradation.

In order to bring the brand-new cells to their desired SoH for creating the combinations of packs listed above, the following types of tests were performed on the batteries at an individual level:

1. Capacity tests - These tests involved Constant Current – Constant Voltage (CC-CV) charging of the cells to 100% State of Charge followed by a constant current discharge to 0% SoC and then a charge to 50% SoC calculated based on the discharged amp hours.
2. Degradation cycling - These involved cyclically charging and discharging the cells at a high C-rate with periodic capacity tests as in 1.

At a series connected pack level, pulse tests were performed. A visual representation of the capacity and degradation tests are shown in a later section; section 2.4.

2.3 Equipment used for the Experiment:

For conducting the experiments, the main components and their roles are briefly described below, followed by a more elaborate elucidation. The following components are involved:

1. Battery Test Equipment - Arbin Instruments Battery Cyclers were used for cell characterization and pulse testing.
2. Temperature Chamber - Test Equity 1000 Series temperature chambers were used to hold the test setup of the batteries for both cell characterization, degradation and pulse testing at a constant temperature.
3. Relay Setup - National Instruments relay setup was used to ensure safety of the series connected battery pack by ensuring the breaking of the circuit in case any of the cell's voltage exceeded the safety limits during testing.
4. 3D Printed Battery Fixtures - Multiple battery fixtures were developed and employed for securing the batteries for experimentation. This included developing fixtures for individual cell characterization and degradation tests (holding one cell) as well as another fixture for holding a pack of 4 cells connected in series.

2.3.1 Battery Test Equipment:

Arbin Instruments Battery Test Equipment was used for cell characterization and degradation as well as Pulse Tests. There were two models involved in the experimentation. One of the Arbin Instruments Battery Tester (S/N 173515) had channels which could support testing batteries only within a voltage range of 0-5V while the second Arbin Instruments Battery Tester (S/N 151843) could support testing with a voltage range of 0-20V. This made them suitable for different types of tests involved in the experiments. The cell characterization and degradation tests were to be done on the Arbin with Voltage range of 0-5V, since the operational voltages for individual cells of both NMC and LFP chemistries were within this range. For the pulse testing of the series connected packs, the Arbin with a voltage range of 0-20V was used. This could hold a maximum of 4 NMC chemistry cells connected in series, and 5 LFP chemistry cells connected in series. In order to ensure a fair comparison of the modeling and experimentation for the two chemistries, it was decided that 4 cells connected in series would be used for both chemistries. The two Arbin Instruments Battery Testers are shown below:

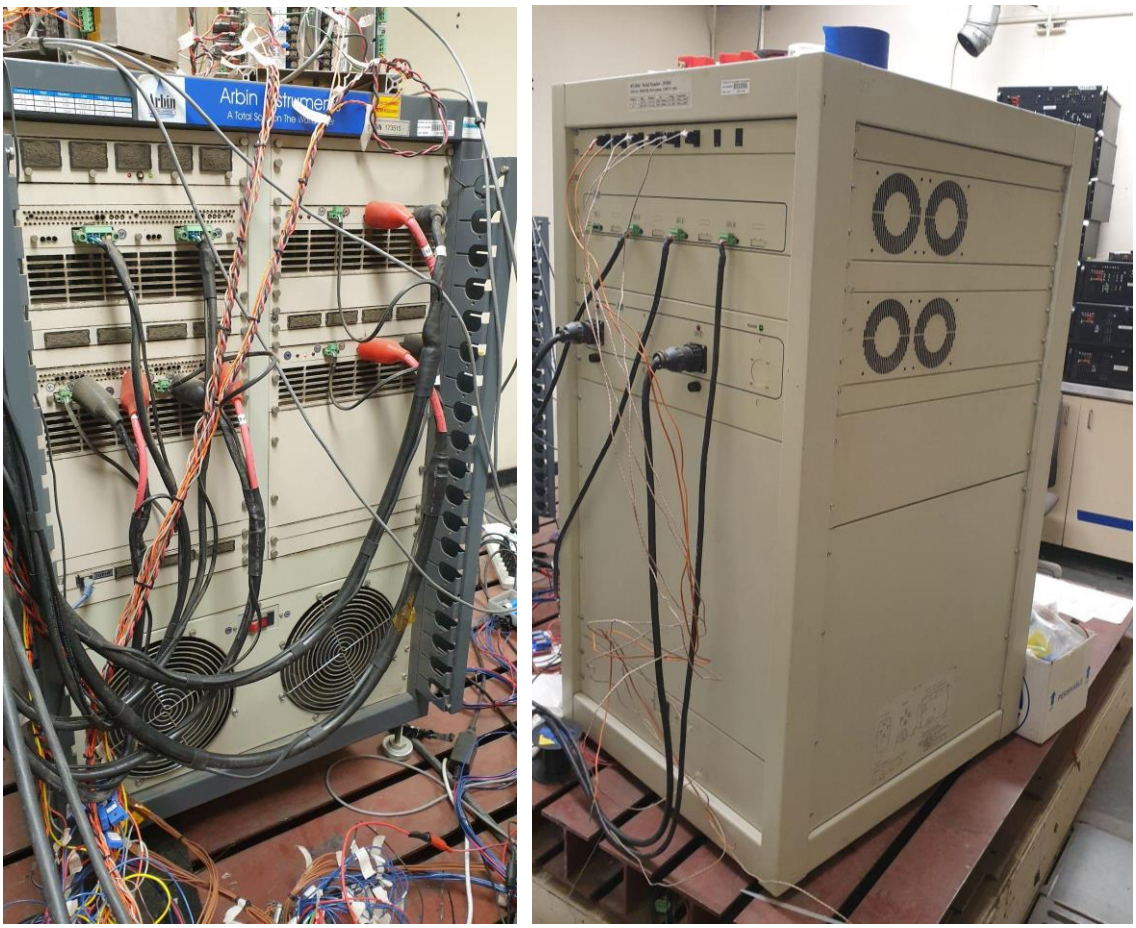

Figure 13: Arbin Instruments Battery Tester (S/N 173515) and (S/N 151843)

Some of the specifications of the Arbin are given below:

Table 4: Specifications of Arbin Instruments Battery Testers

	Arbin S/N 173515		**Arbin S/N 151843**	
Channel #	**Current Range**	**Voltage Range**	**Current Range**	**Voltage Range**
Channel 1,2	±20A	0-5V	±5A	0-20V
Channel 3,4	±50A	0-5V	±5A	0-20V
Channel 5,6	±100A	0-5V	±20A	0-20V

2.3.2 Temperature Chamber:

TestEquity 1000 Series Temperature Chamber was used for conducting all the experiments. As mentioned in [3], temperature can have a profound effect on the nature of degradation of the cells and therefore, it was important to ensure that the degradation as well as the cell characterization tests were conducted at a constant temperature. The chamber was therefore subsequently used for all tests for both the NMC and LFP chemistries of cells. An image of the temperature chamber used is shown in fig. 14 below:

Figure 14: TestEquity Temperature Chamber

The specifications of the temperature chamber from the manufacturer are provided in Appendix A.

2.3.3 Relay Setup:

During the testing operation of the series connected battery packs, the Arbin Battery Tester did not directly receive the voltage measurements from the individual cells. Hence, an additional system was installed in order to break the circuit in case any one of the 4 cells exceeds its safe voltage operation limits. This was achieved by using a relay system from National Instruments (NI). The positive terminal of the Arbin was first connected to the Relay, which was a NI 9472 module. The individual voltage readings were taken from the NI 9205 module as shown in fig. 15. In case any one of the cell voltages exceeded the safety limits, then it was communicated to the Relay module which immediately opened the circuit and stopped further current charge/discharge from taking place.

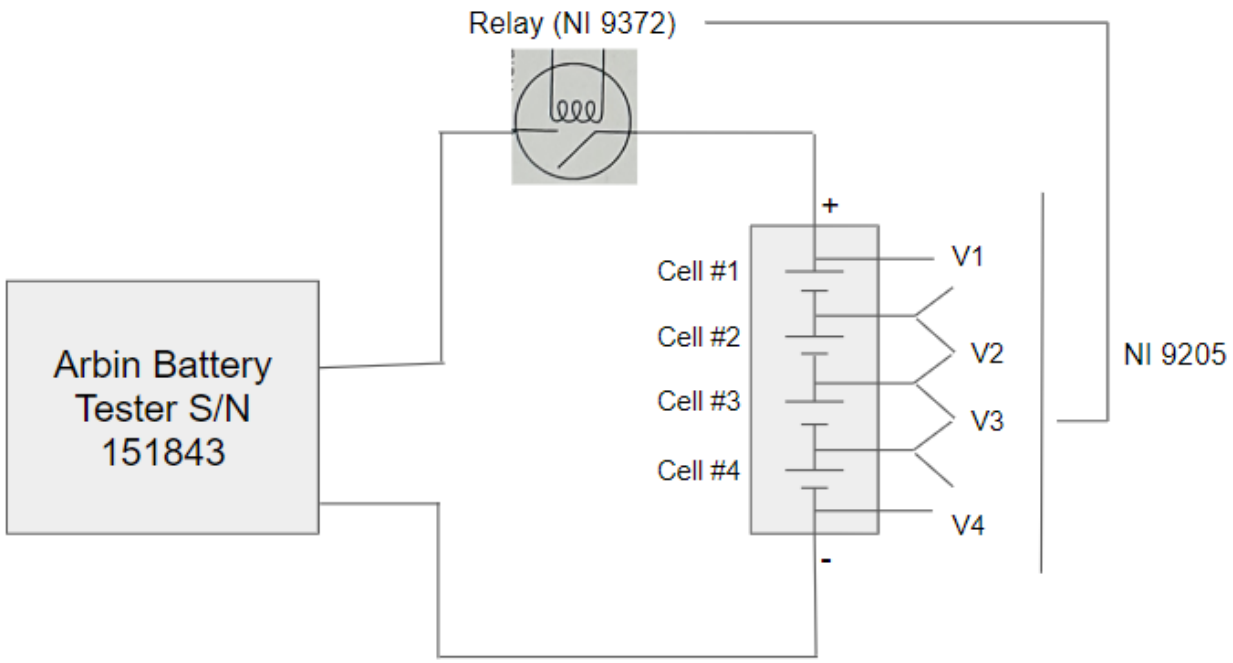

Figure 15: Relay system schematic

2.3.4 3D Printed Battery Fixtures

Battery testing modes 1. and 2. from section 2.2 were employed for single individual cells while the pulse tests were performed for a series connected pack consisting of 4 cells and therefore, different fixtures were required for the individual and pack level experiments. As a 3D printer was available, it was possible to iterate designs for both types of fixtures. The 3D printer model was a Prusa Original i3 MK3S+ for which both ABS and PLA filaments were used for 3D printing the fixtures. The 3D printer used is shown below in fig. 16:

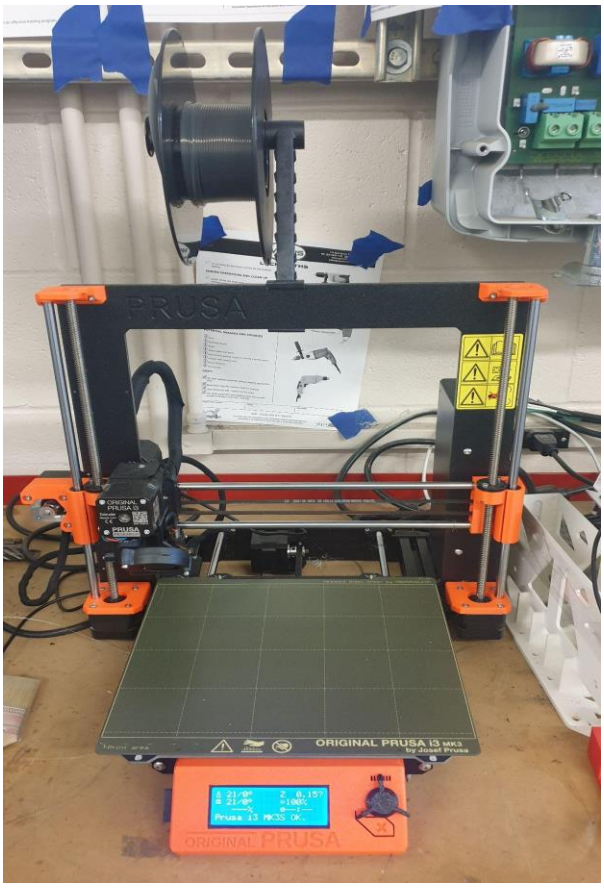

Figure 16: Prusa Original i3 MK3S+ 3D Printer

The specifications of the 3D printer from the manufacturer are provided in Appendix B.

The development of the 3D printed fixtures was an iterative process with the following goals under consideration:

1. Consistent pressure on the battery-bus bar contact patch
2. Ergonomics - ease of insertion and removal of cells
3. Minimal usage of 3D printer filament

With these objectives in mind, upon successive iterations the following fixture was designed for the individual cells:

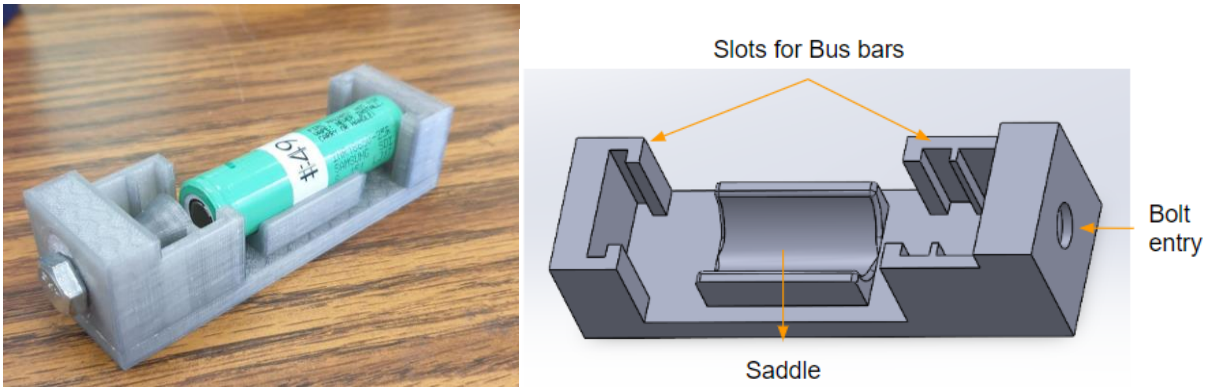

Figure 17: Single cell fixture 3D printed and its CAD model

The key features of this design were as follows: The shape of the fixture was somewhat derived from that of a C-clamp. The cell rested on a saddle to secure its lateral movement. There were slots provided at both terminal ends for smoothly sliding the copper bus bars into position, which came from the Arbin. To secure the copper bus bars into position throughout the tests, a nut and bolt mechanism was devised to apply pressure on the battery-bus bar contact and hold them in their places through friction. On the wall at the thicker end, a circular hole was provided through which a bolt could enter. A slot in the shape of a nut was extruded just beyond the circular hole inside the walls of the fixture as shown in fig. 18. The nut had snug fit into the slot, and once the bolt had been inserted, it could simply be rotated clockwise to tighten its way into the fixture. At the end of the bolt, a threaded cap was screwed onto it such that it applied pressure over a greater area onto

the copper bus bars, whilst pushing it in towards the battery and securing the setup as shown in fig. 18. Upon multiple iterations the length of the fixture was determined which would keep consistent and optimal pressure on the battery-bus bar setup based on the criteria of mentioned above.

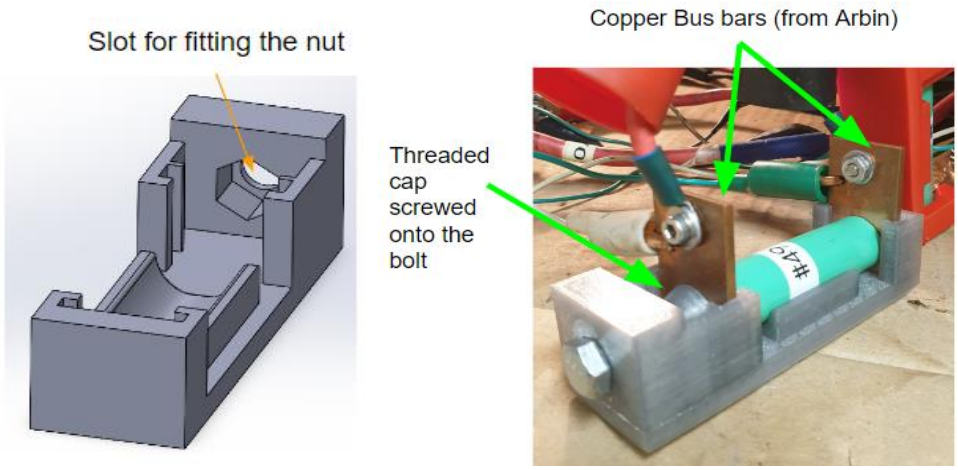

Figure 18: Single cell fixture CAD model and fixture in operation

When it came to the pack fixtures, the same design was simply extended to 4 cells in series as shown in fig. 19. The copper bus bars ensured that the series configuration was established, and the set of common terminals are marked in green, yellow and orange in fig 19.

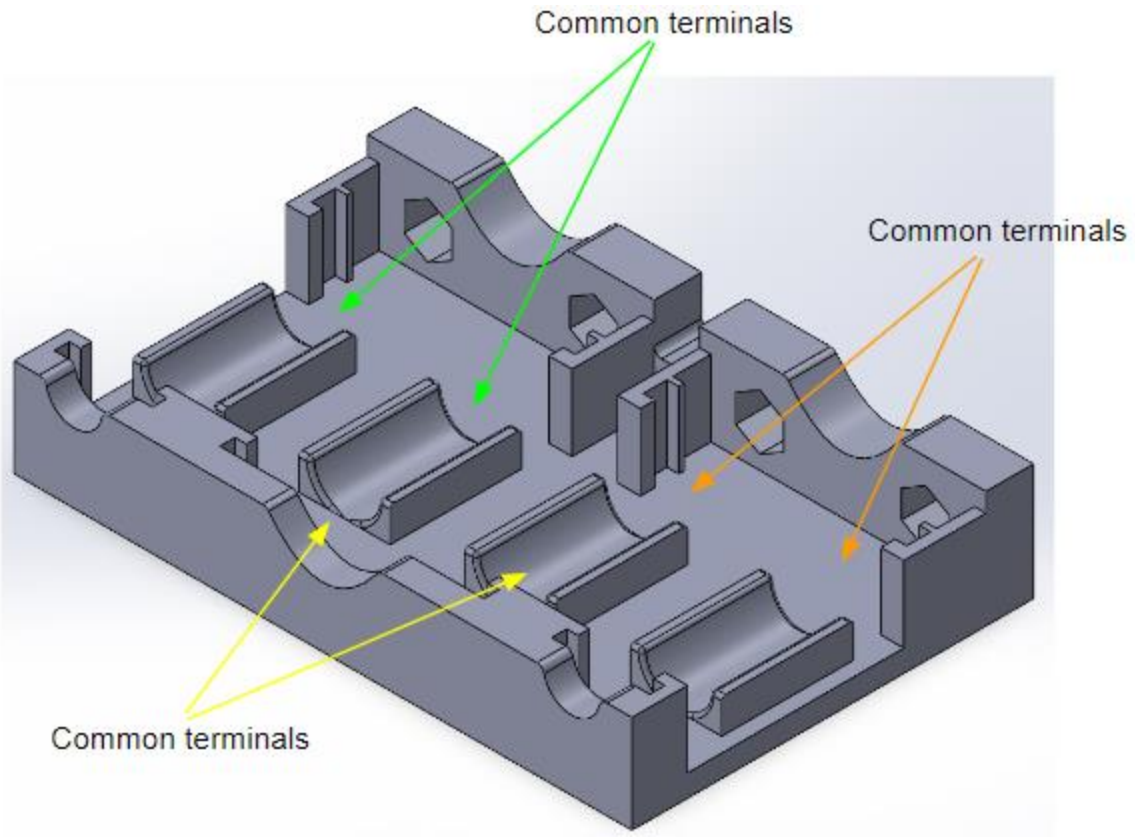

Figure 19: CAD model of pack fixture showing the common terminals

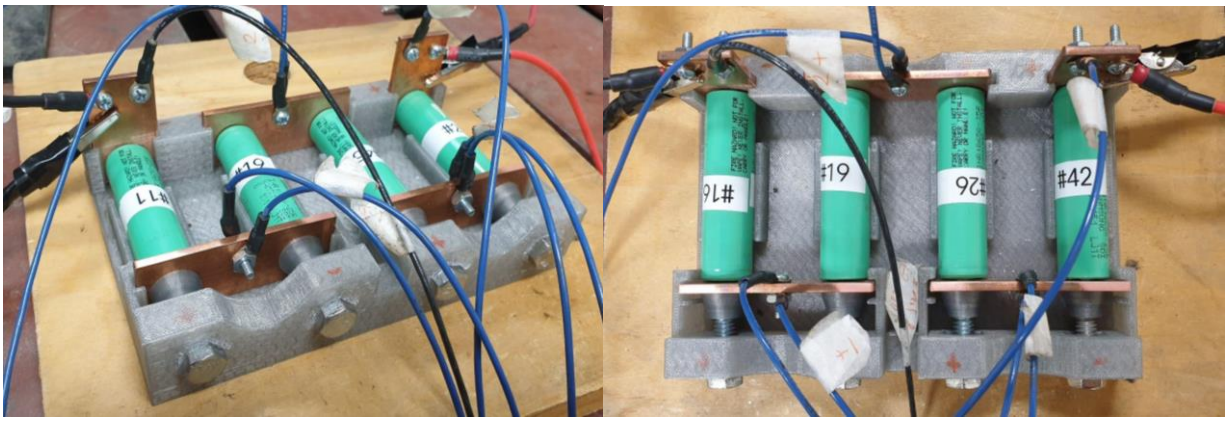

Figure 20: Pack fixture in operation

The above figure (fig. 20) shows the actual setup of the cells and clearly depicts which of the cells shared a common terminal. Also note the orientations of each of the cells, indicating their correct configurations in forming a series connection from the first to the last cell.

2.4 Degradation of the Cells

All the LFP and NMC chemistry cells were degraded in an identical manner from their time of purchase. The only consideration was that the LFP cells have an additional 12 months of calendar aging over the NMC chemistry of cells, as these were available from a previous batch of purchased cells. However, since all the LFP cells experienced uniform calendar aging the effect could be neglected for the purpose of the experiments. Flowcharts to describe the capacity tests for NMC and LFP tests are shown below. Note that the tests also involved charging the cells up to 50% of the calculated discharge capacity from the same test, in order to have the cells ready for the subsequent pulse testing experiments.

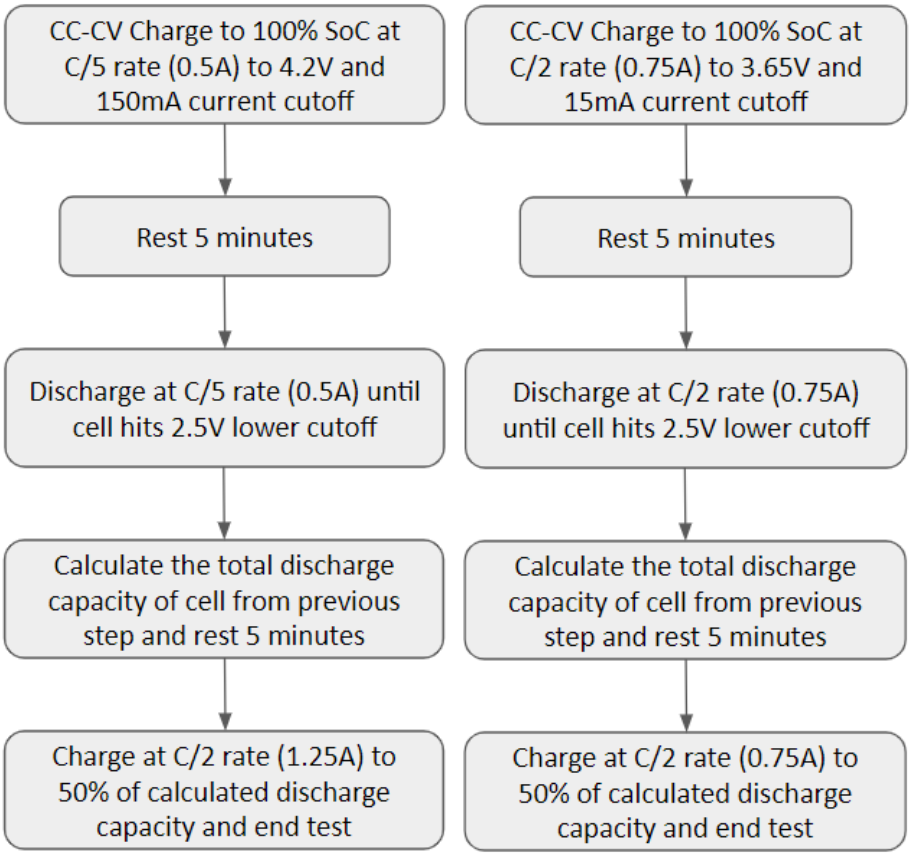

Figure 21: Capacity tests flowchart: for NMCs (left) and LFPs (right)

The degradation of the cells followed a similar procedure, and it is described in the following flowcharts. Note that there was a threshold of up to 1.5% above the proposed SoH since a slight variability in the battery SoH was desired.

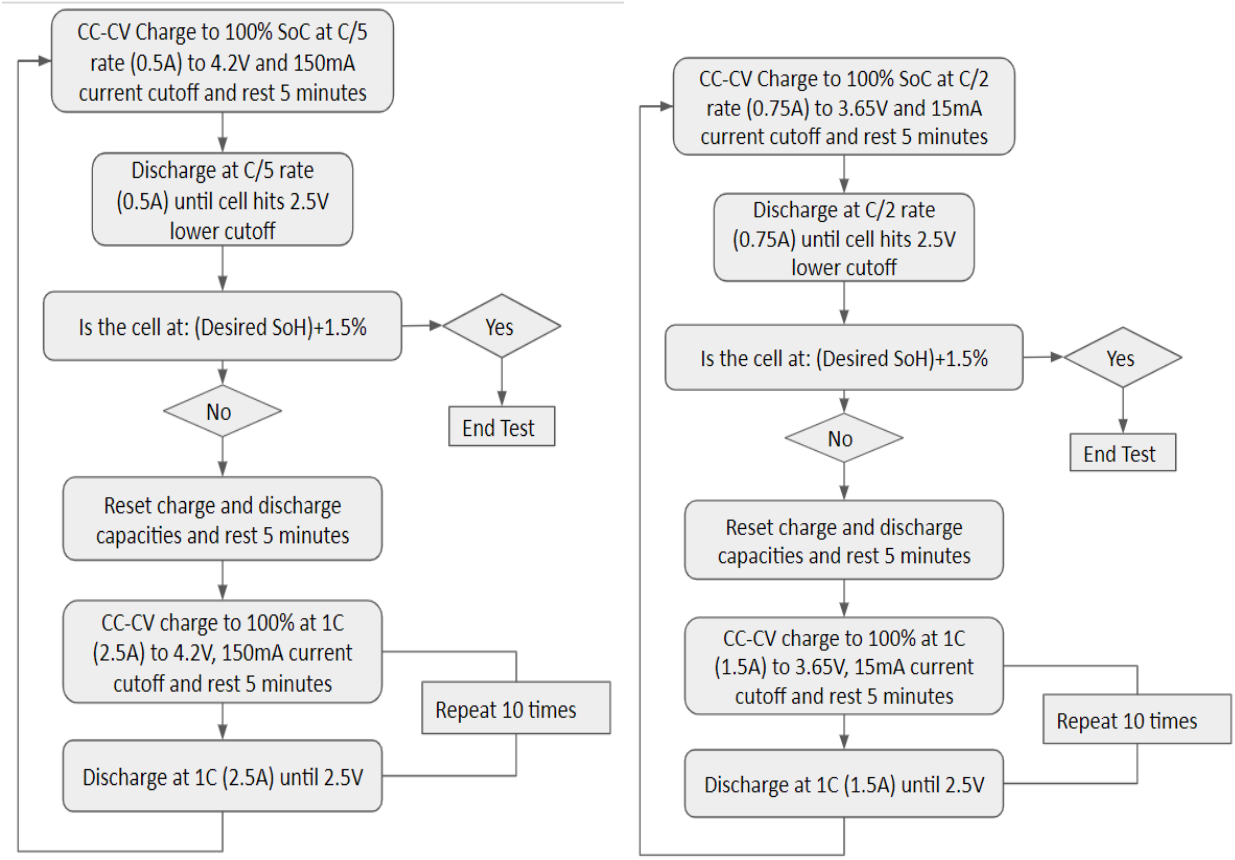

Figure 22: Degradation cycling: for NMCs (left) and LFPs (right)

The final LFP cells used for the experiments had the following State of Health, listed in order of decreasing ‘proposed SoH’.

Table 6: Final SoH of LFP cells used in the experiment

Cell Number	Proposed SoH	Actual SoH	Deviation from Proposed
C13	95%	94.72%	0.3%
C16	95%	95.15%	-0.2%
C67	95%	95.06%	-0.1%
C51	95%	95.24%	-0.2%
C02	95%	94.80%	0.2%
C28	90%	90.67%	-0.7%
C44	90%	90.56%	-0.6%
C55	90%	89.43%	0.6%
C62	85%	86.00%	-1.0%
C21	85%	87.34%	-2.3%
C41	85%	84.10%	0.9%
C14	80%	82.02%	-2.0%
C65	80%	80.11%	-0.1%
C12	80%	80.14%	-0.1%

The NMC cells used for the experiments had the final SoH distribution, listed in order of decreasing ‘proposed SoH’:

Table 7: Final SoH of LFP cells used in the experiment

Cell Number	Proposed SoH	Actual SoH	Deviation from Proposed
C11	95%	94.88%	0.1%
C16	95%	93.83%	1.2%
C17	95%	95.45%	-0.5%
C19	95%	95.69%	-0.7%
C45	95%	94.77%	0.2%
C10	90%	91.08%	-1.1%
C21	90%	91.14%	-1.1%
C40	90%	91.39%	-1.4%
C12	85%	86.54%	-1.5%
C13	85%	85.74%	-0.7%
C49	85%	85.95%	-1.0%
C14	80%	81.21%	-1.2%
C26	80%	81.65%	-1.7%
C42	80%	80.43%	-0.4%

This concludes chapter 2, which introduced the experimental methodology, the equipment used, specifications and properties of the cells used, degradation and capacity test descriptions and finally, the SoH of the cells used in the experiments. The next chapter introduces the preliminary tests which formed the basis for the final pulse tests used in the rapid SoH estimation model.

Chapter 3: Preliminary Pulse Tests

3.1 Pulse Test Description

The final pulse test experiment design was based on the results of the preliminary pulse tests whereby multiple pulses with different current magnitude and time duration were applied to randomly selected series connected battery packs for both the NMC and LFP chemistries. As per [28] where the effect of pulse magnitude and duration was studied for estimation of ECM parameters, it was found that the higher the current magnitude, the better the parameter estimation accuracy, whereas beyond a certain pulse duration, the estimation accuracy could not improve.

In order to first ascertain that the findings of [28] would be applicable to total SoH estimation modeling, and subsequently determining the pulse magnitude and duration required for total SoH estimation, the preliminary pulse tests were conducted. The outcomes of these preliminary pulse tests would be used to determine the minimum pulse duration that would be needed as well as to establish that higher pulse magnitude led to better total SoH estimation.

The time scales of 1 second, 10 seconds and 1 minute for the charge and discharge pulses were initially tested. Moreover, these were conducted with magnitudes of 0.5C and 1C for each chemistry. For reference, this type of pulse testing is described as the Hybrid Pulse Power Characterization (HPPC) test in industry and is mainly used for establishing the power capabilities of a cell. However, later on several studies have used this technique to also estimate ECM parameters of cells. The applied current pulse in the preliminary tests is shown in fig. 23 below:

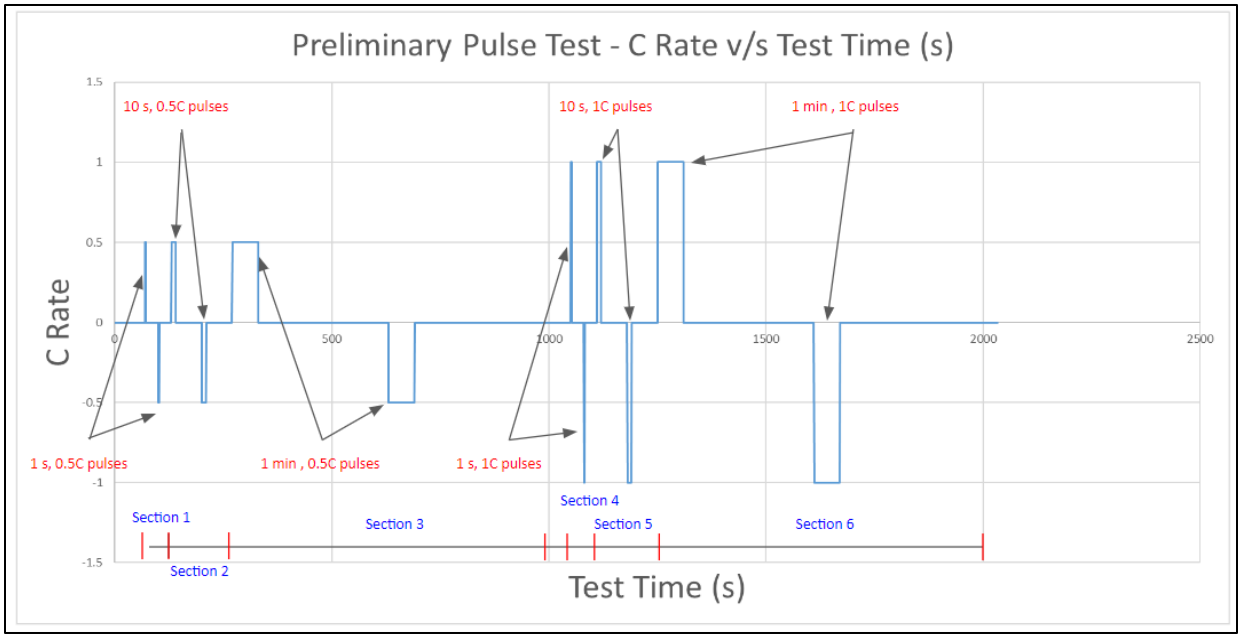

Figure 23: Preliminary Pulse Test - C Rate v/s Test Time (s)

The preliminary test pulse is described as follows:

1. 70 second initial rest - to ensure all cells are at a stable voltage
2. 1 second, 0.5C charge and discharge pulses, separated by 30 seconds of rest
3. 30 seconds of rest
4. 10 second, 0.5C charge and discharge pulses, separated by 1 minute of rest
5. 1 minute of rest
6. 1 minute, 0.5C charge and discharge pulses, separated by 5 minutes of rest
7. 6 minutes of rest - then repeat of the previous steps with 1C current pulses as follows:
8. 1 second, 1C charge and discharge pulses, separated by 30 seconds of rest
9. 30 seconds of rest
10. 10 second, 1C charge and discharge pulses, separated by 1 minute of rest
11. 1 minute of rest
12. 1 minute, 1C charge and discharge pulses, separated by 5 minutes of rest

Note that for the NMC cells, 0.5C and 1C corresponds to 1.25A and 2.5A respectively, whereas for the LFP cells, 0.5C and 1C corresponds to 0.75A and 1.5A, respectively. For convenience, the sections of the pulses are designated into sections 1 through 6 as depicted in the figure above (fig. 23), where sections 1, 2 and 3 are of the 0.5C pulses with time durations of 1s, 10s and 1 minute, respectively. Sections 4, 5 and 6 are of the 1C pulses with time durations of 1s, 10s and 1 minute, respectively. This described in the table below:

Table 8: Preliminary Pulse Test Section Description

Section #	Pulse Current magnitude	Pulse time duration
Section 1	0.5C	1 second
Section 2	0.5C	10 seconds
Section 3	0.5C	1 minute
Section 4	1C	1 second
Section 5	1C	10 seconds
Section 6	1C	1 minute

Note that in addition to the pulses themselves, the sections also include the rest period between the current pulses as is shown fig. 23.

3.2 Pulse Test Results

3.2.1 Results of the preliminary pulse testing on NMC packs:

There were 6 packs used for this preliminary experiment chosen at random from the available/possible combinations of series connected battery packs. These consisted of 1 each of: Ideal pack, 1C90, 1C80, 2C80, along with two 1C85 packs. The voltage response of the 6 packs is shown in the figure below:

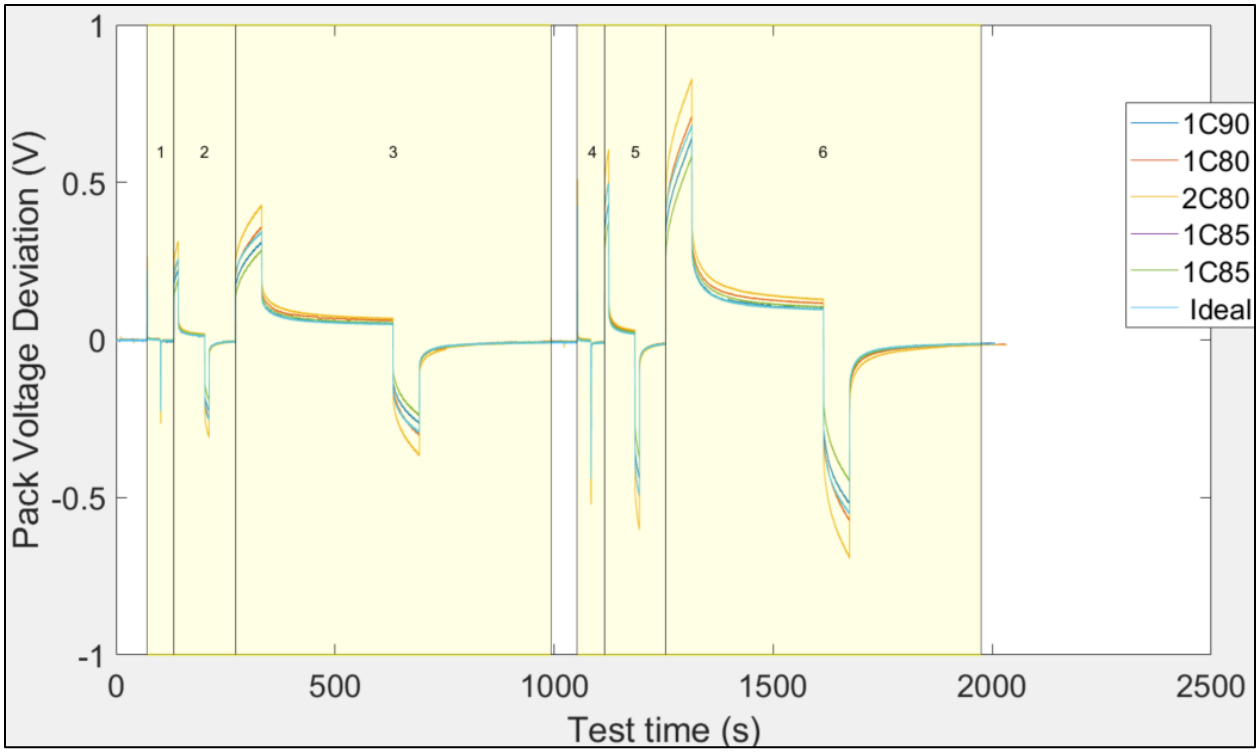

Figure 24: Preliminary Pulse Test - NMC packs Raw Data

The x-axis represents the test time, and the y-axis shows the voltage deviation of each pack from its own voltage at the start of the test. By visual inspection it was clear that the largest magnitude of response is of the 2C80 pack, which was expected since it would have a greater difference in SoH compared to all other packs. However, the rest of the pulses were somewhat closer together, indicating that the role of higher order dynamics did have an influence on the SoH and therefore, the response of the packs to such current pulses. In order to establish a preliminary statistical relationship between the actual SoH and correlation between the various pulses, the following three parameters were determined from the pulse tests. They are as follows:

1. DCIR - Direct Current Internal Resistance is the instantaneous voltage change of a cell/pack to the application of current. Note that this parameter can be calculated independent of any other test and can be conducted at every pulse individually.

2. RMSD - Root Mean Square Difference is the root of the mean of the squared difference between the voltage deviation of a given test with respect to a reference test over the corresponding time steps. It is given by:

$$\text{RMSD} = \sqrt{\frac{\sum_{i=1}^{N}(Vref_i - Vtest_i)^2}{N}}$$

Where $Vref$ - voltage deviation of reference test

$Vtest$ - voltage deviation of given test

N - number of data points/time steps

3. MAPD - Mean Absolute Percentage Difference: It is the percentage of the average difference in the voltage deviation between the given test and a reference test with respect to the reference test. It is given by:

$$\text{MAPD} = \frac{1}{N}\sum_{i=i}^{N}\left|\frac{Vref_i - Vtest_i}{Vref_i}\right| \times 100\%$$

Where $Vref$ - voltage deviation of reference test

$Vtest$ - voltage deviation of given test

N - number of data points/time steps

It must be noted that the Arbin Battery Tester was programmed to record data at 100Hz or every 10 milliseconds. For the voltage deviation in all tests to be at the same time step for the statistical analysis, the raw data was modified by rounding to the nearest one hundredth of a second (10ms). Furthermore, in addition to the calculation of the above parameters over the entire test duration, these parameters were calculated for each of the 6 sections as well. This was important to proceed with developing the final pulse tests discussed in Chapter 4.

The sectional and overall statistical parameters were calculated for the 6 tests. The correlation coefficient between the total SoH and each of DCIR, RMSD and MAPD was calculated, which is a statistical measure of the strength of the relationship between two variables.

In addition, the p-values of the corresponding relationships were also calculated. In simple terms, the p-values denote the probability of an observed relation arising from random chance. Therefore, for the relationship between two variables to be statistically significant, the p-value must be as low as possible. The commonly accepted threshold for statistical significance with 95% confidence is for the p-value to be less than 0.05. As mentioned in section 3.1, the findings of [28] suggest that the higher C-rates, i.e., sections 4-6 would yield stronger relationships compared to sections 1-3. Furthermore, sections 2 and 3 would yield stronger relationships than section 1, and similarly, sections 5 and 6 would yield better relationships than section 4 since the pulse duration was longer. The correlation coefficients and corresponding p-values (in parenthesis) for the dataset of the 6 preliminary tests are shown in the table below. Note that '***' corresponds to a 0.0001 level of significance, '**' to 0.001, and '*' to 0.01 level of significance:

Table 9: Correlation Coefficients and p-values between Total SoH and DCIR, RMSD and MAPD

	Total SoH ~ DCIR	**Total SoH ~ RMSD**	**Total SoH ~ MAPD**
Overall	-0.99226 *** (0.00081681)	-0.5006 (0.39034)	-0.99652 *** (0.00024667)
Section 1	-0.8148 * (0.092971)	-0.052458 (0.93324)	0.55342 (0.3332)
Section 2	-0.791 (0.11103)	-0.78817 (0.11324)	-0.77264 (0.12561)
Section 3	-0.83138 * (0.08098)	-0.97903 ** (0.0036338)	-0.96495 ** (0.0078352)
Section 4	-0.83876 * (0.075816)	-0.71041 (0.17872)	0.98771 ** (0.0016334)
Section 5	-0.84812 * (0.069415)	-0.73885 (0.15377)	-0.99993 *** (0.00000064777)
Section 6	-0.83062 * (0.081519)	-0.97468 ** (0.0048171)	0.31439 (0.6064)

As observed from table 9 containing p-values, there was statistical significance for the Total SoH ~ MAPD for half of the sections, as well as the overall test. There was statistical significance for the Total SoH ~ RMSD relation only for sections 3 and 6. In the case of the Total SoH ~ DCIR relation, there was no statistical significance at any of the individual sections, and hence we could not consider it for determining the final test pulse profile. Looking at the correlation coefficients, there was excellent correlation between Total SoH ~ MAPD at overall test level as well as at sections 3, 4 and 5. In terms of the Total SoH ~ RMSD relation the correlation coefficient was excellent for sections 3 and 6. It was also observed that the correlations were stronger for the 1C pulses compared to the 0.5C pulses. Furthermore, the correlations improve with increasing pulse duration from 1s to 10s, and it was highest for a 10s pulse which also has the lowest p-value.

3.2.2 Results of the preliminary pulse testing on LFP packs:

A similar exercise was also carried out on the LFP chemistry of cells using the same parameters for statistical analysis. Here, the tests were carried out on a slightly larger sample space of randomly chosen battery pack combinations. This included two ideal packs, one 1C90 pack, three 1C85 packs, one each of 1C80 and 2C85 packs. The voltage responses of the pulse tests on the LFP cells are shown in fig. 25 below:

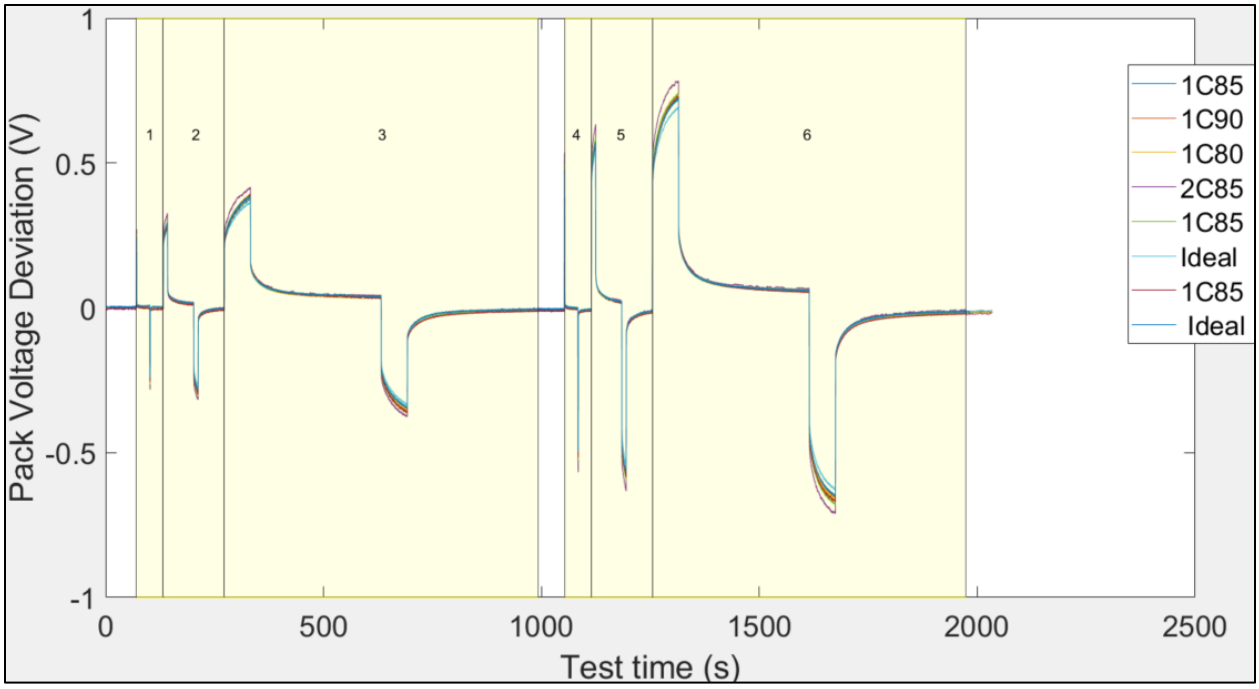

Figure 25: Preliminary Pulse Test - LFP packs Raw Data

The sectional and overall statistical parameters were calculated for the 8 tests. Again, as mentioned in sections 3.1 and 3.2.1, the findings of [28] suggest that the higher C-rates, i.e., sections 4-6 would yield stronger relationships compared to sections 1-3. Furthermore, sections 2 and 3 would yield stronger relationships than section 1, and similarly, sections 5 and 6 would yield better relationships than section 4 since the pulse duration was longer. The correlation coefficients and corresponding p-values for the dataset of the 6 preliminary tests are shown in the table below. Again, note that '***' corresponds to a 0.0001 level of significance, '**' to 0.001, and '*' to 0.01 level of significance:

Table 10: Correlation Coefficient between Total SoH and DCIR, RMSD and MAPD

	Total SoH ~ DCIR	**Total SoH ~ RMSD**	**Total SoH ~ MAPD**
Overall	-0.93031 ** (0.0023715)	-0.58793 (0.16504)	-0.17721 (0.70386)
Section 1	-0.71026 * (0.073707)	-0.0077182 (0.9869)	0.11665 (0.80331)
Section 2	-0.77513 * (0.040629)	-0.12263 (0.79338)	-0.43109 (0.33422)
Section 3	-0.82662 * (0.021846)	0.031037 (0.94734)	0.12405 (0.79103)
Section 4	-0.84789 * (0.015941)	-0.020121 (0.96585)	-0.19219 (0.67973)
Section 5	-0.85702 * (0.013726)	-0.41104 (0.35962)	0.010711 (0.98182)
Section 6	-0.86501 * (0.01194)	-0.84983 * (0.015454)	0.36007 (0.42757)

It could be observed that there was no statistically significant relation between total SoH and either of RMSD or MAPD, except for the RMSD in section 6, where the p-value was ~0.015 with a correlation coefficient of -0.85. However, barring section 1, in all remaining sections there was a statistically significant relationship between total SoH and DCIR. Like the NMC battery packs, the relationship was stronger for the 1C pulses compared to the 0.5C pulses, and it got stronger when the pulse duration was increased, especially from 1s to 10s. There was a slight increase in the correlation coefficient going from 10s to 1 minute as well, but it was a marginal increase as seen from table 10.

This concludes chapter 3 discussing the preliminary pulse tests undertaken which formed the basis for the final pulse test design, discussed in chapter 4.

Chapter 4: Final Test Pulse - Results and Discussion

4.1 Inferences from the Preliminary Pulse Tests on the NMC and LFP chemistry:

1. As the current pulse magnitude was increased from 0.5C to 1C, there was a clear increase in the statistical significance and correlation between the total SoH and the parameters for both NMC and LFP chemistries.
2. As the pulse duration was increased from 1s to 10s, there was a clear increase in the statistical significance and correlation between the total SoH and the parameters again for both chemistries.
3. The increase in the strength of the correlation as the pulse duration was increased from 10s to 1 minute, was marginal in case of the total SoH ~ DCIR relationship for the LFP chemistry, while it was less obvious in case of the NMC chemistry, since the MAPD relationship deteriorated, RMSD improved and the DCIR was just about marginal.

These inferences were consistent with the observations of [28] where the experiments were performed on a single cell to estimate the parameters of a 2^{nd} order ECM model using pulse tests. Increasing current magnitude always improved estimation accuracy while increasing the pulse duration beyond a certain time period of about 10 seconds did not improve the estimation accuracy.

4.2 Final Pulse Test Description

Based on the observations in Chapter 3, inferences listed in section 4.1 and the fact that these matched with the results from [28], the following pulse test was designed for the final experiment, corresponding to sections 2 and 5 in the preliminary tests from Chapter 3:

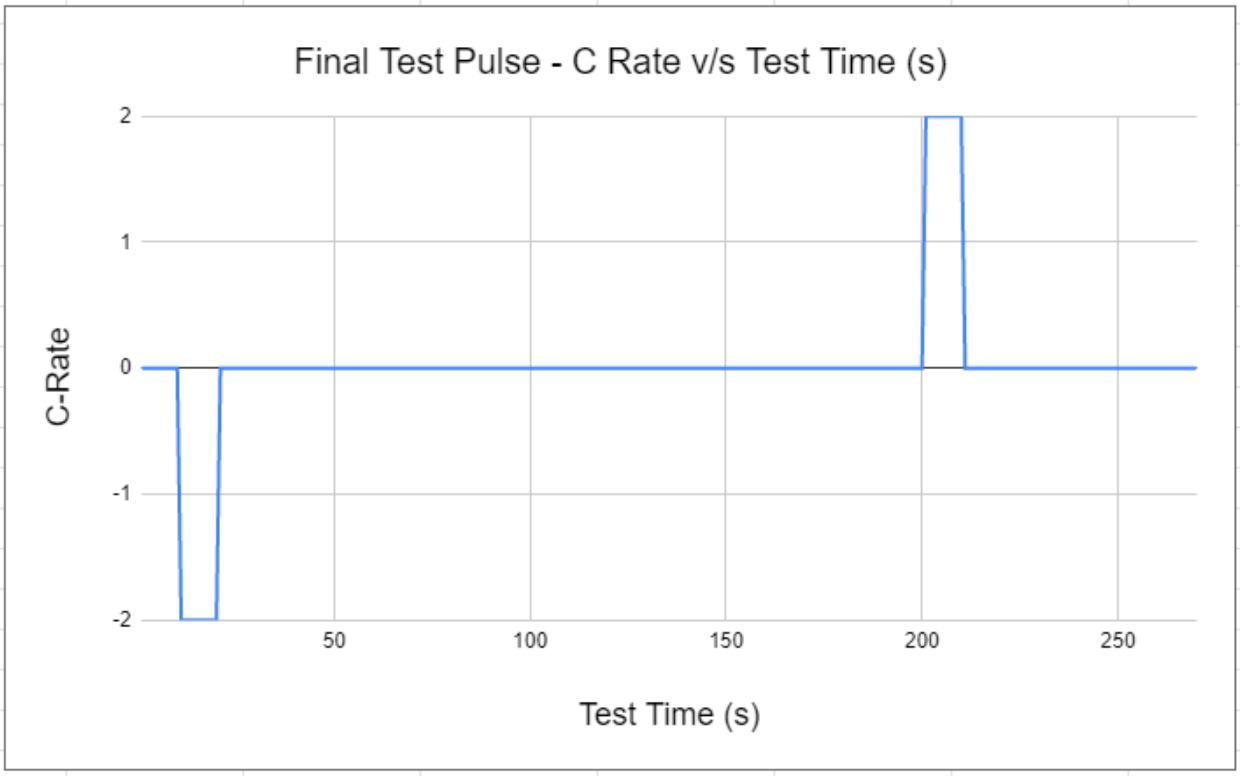

Figure 26: Final Test Pulse - C Rate v/s Test Time (s)

The final pulse test was much shorter and simpler than the preliminary pulse test whilst incorporating the findings of Chapter 3. It was as follows:

1. Initial 10 second rest
2. 10 second, -2C discharge pulse
3. 3-minute rest period
4. 10 second, 2C charge pulse
5. 70 seconds rest period

Note that the current magnitude was further increased to 2C for the final pulse tests which was above the magnitude tested in the preliminary tests from Chapter 3. This was in line with inference 1. and [28], which implied that increasing current pulse magnitude improved the estimation accuracy. The reason for not increasing beyond 2C magnitude was that it was the maximum allowable charge C-rate for the LFP cells as per the manufacturer. Also note that the 2C current magnitude corresponds to 5A for NMC cells and 3A for the LFP cells. The pulse duration was limited to 10 seconds since there was only marginal improvement in the statistical relationship between the total SoH and the three parameters, based on inferences 2. and 3. In addition, this also aligned with the motivation of the project to have short pulses in a quick test to determine the total SoH of a given battery pack as well.

4.3 Initial Results on NMC and LFP chemistries:

The number of packs on which the pulse tests were performed are as follows:

Table 11: Pack type and corresponding number of tests conducted – NMC chemistry

Pack Type	**Number of Packs Tested**
Ideal	5
1C90	16
1C85	14
1C80	14
2C90	14
2C85	15
2C80	15
Total	93

The results of the NMC cells were:

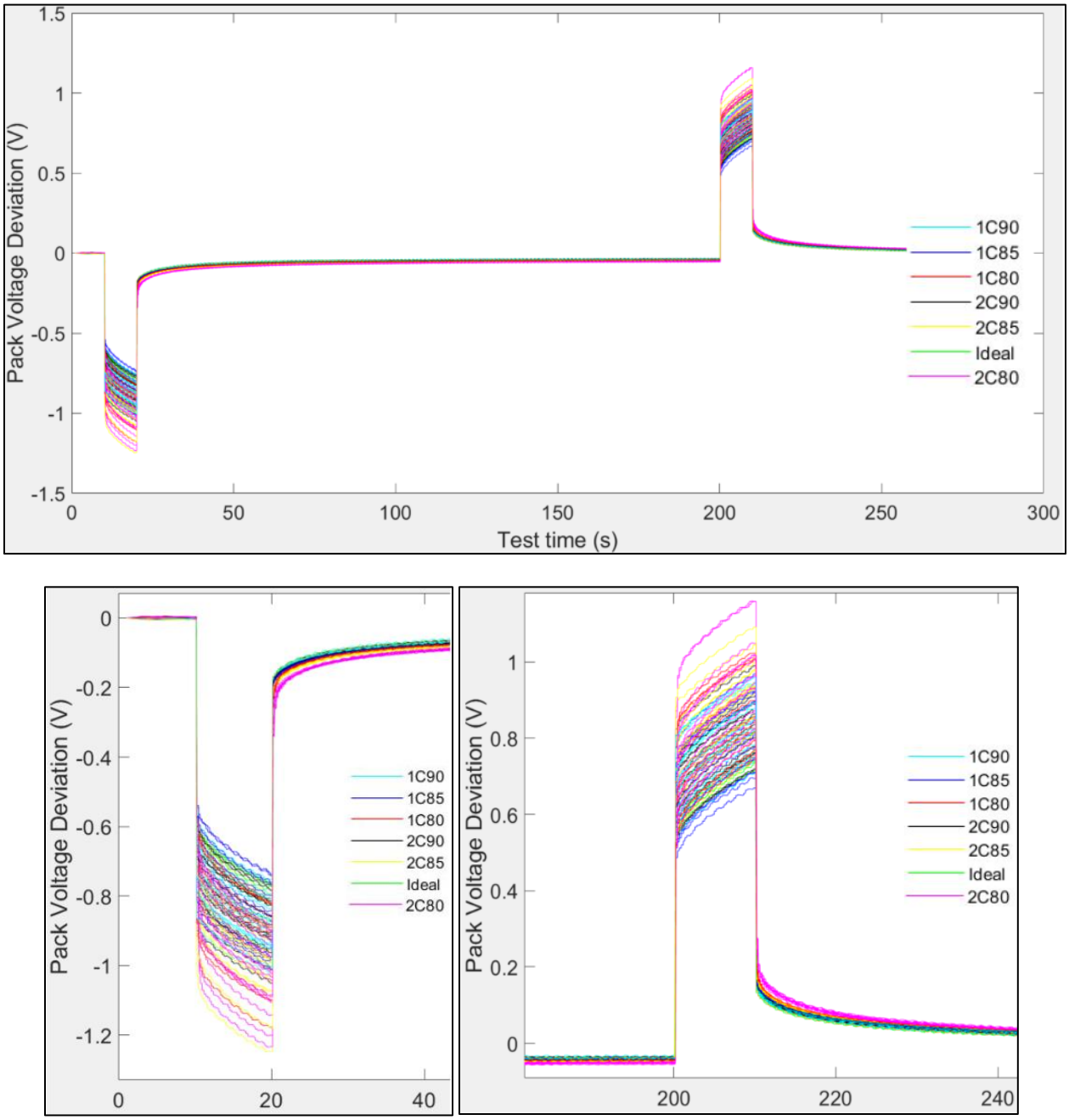

Figure 27: Final Pulse test for NMC packs - Raw results: Top – full test duration, Bottom left – expanded view of discharge pulse (x-axis – test time) and Bottom right – expanded view of charge pulse (x-axis – test time)

As clear from fig. 27, the 2C80 packs showed the greatest voltage response while the remaining packs showed progressively lower deviation, although an overlap between different packs was also clearly visible. The three parameters applied in Chapter 3 were also applied here on the overall pack and the correlation coefficients and corresponding p-values are shown in the table below:

Table 12: Correlation Coefficients and p-values for Total SoH v/s DCIR, RMSD, MAPD

Relation	**Correlation Coefficient**	**p-value**
Total SoH ~ DCIR	-0.4698	2.03E-06
Total SoH ~ RMSD	-0.4838	8.97E-07
Total SoH ~ MAPD	-0.9503	6.52E-48

It was clear that all three relationships had statistical significance since their p-values are <<0.05. Even though the p-values for all three relationships was nearly zero, in particular, the relationship Total SoH ~ MAPD had an exceptionally low p-value of the order of magnitude of 10^{-48} indicating a potentially stronger relationship of the Total SoH with MAPD versus the other parameters. This was reflected in the high correlation coefficient of -0.95, compared to the relatively lower values of -0.46 and -0.48 for the DCIR and RMSD relationships, respectively. The plot of Total SoH versus MAPD, RMSD and DCIR is shown below which visually confirmed the strong correlation.

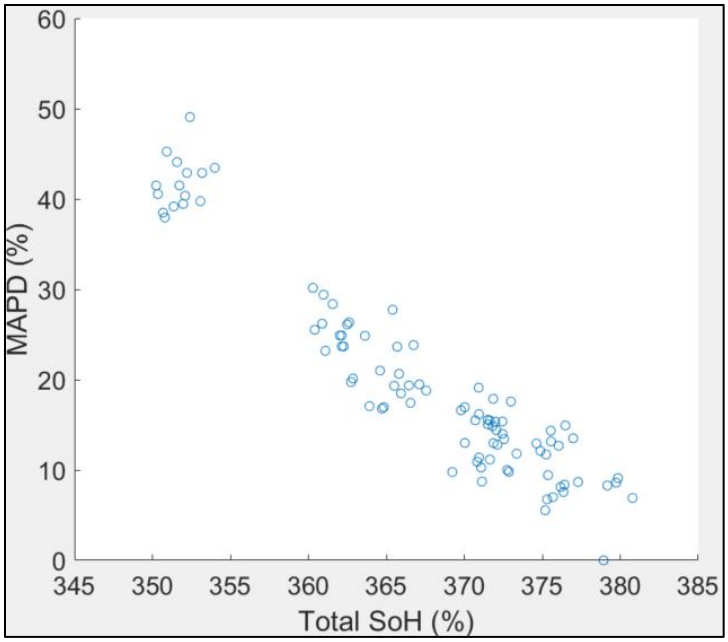
MAPD (%)
Total SoH (%)
0
10
20
30
40
50
60
345
350
355
360
365
370
375
380
385

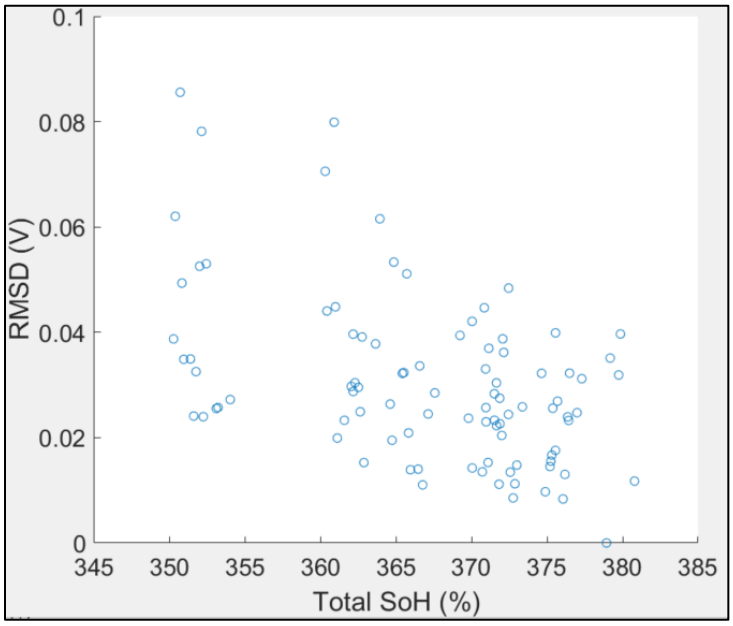
RMSD (V)
Total SoH (%)
0
0.02
0.04
0.06
0.08
0.1
345
350
355
360
365
370
375
380
385

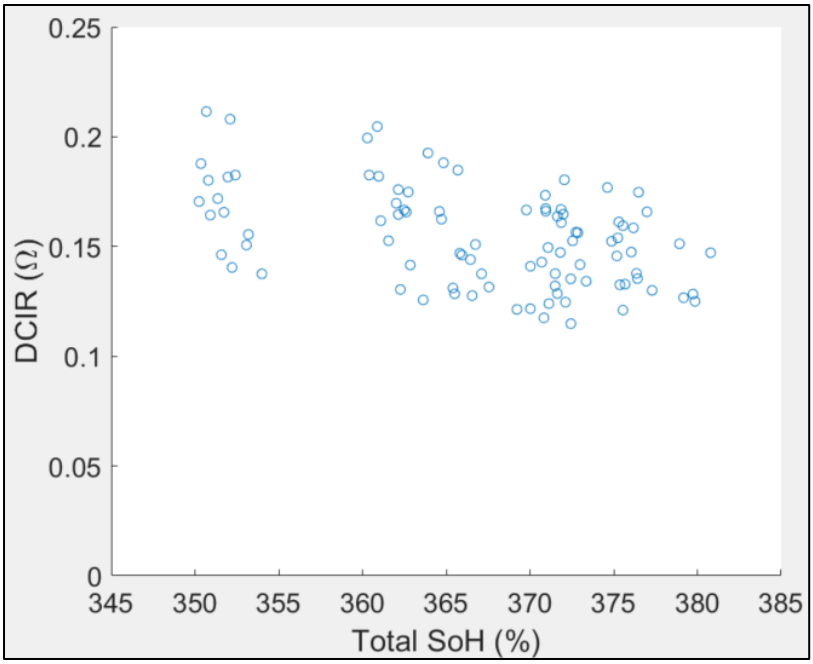

Figure 28: Top -MAPD (%) v/s Total SoH %, Center - RMSD (V) v/s Total SoH %, Bottom – DCIR (Ω) v/s Total SoH %, over 93 NMC pack tests

It was clear from fig. 28 that there existed an almost linear relationship between the Total SoH and the MAPD of a given test. Note that the x-axis representing the Total SoH is truncated between 345-385% as it encompassed the entire range of possible SoH. Next, the analysis of the LFP tests was carried out. The number of packs on which the pulse tests were performed are as follows:

Table 13: Pack type and corresponding number of tests conducted – LFP chemistry

Pack Type	Number of Packs Tested
Ideal	5
1C90	16
1C85	16
1C80	16
2C90	15
2C85	16
2C80	15
Total	99

The results of the LFP cells were:

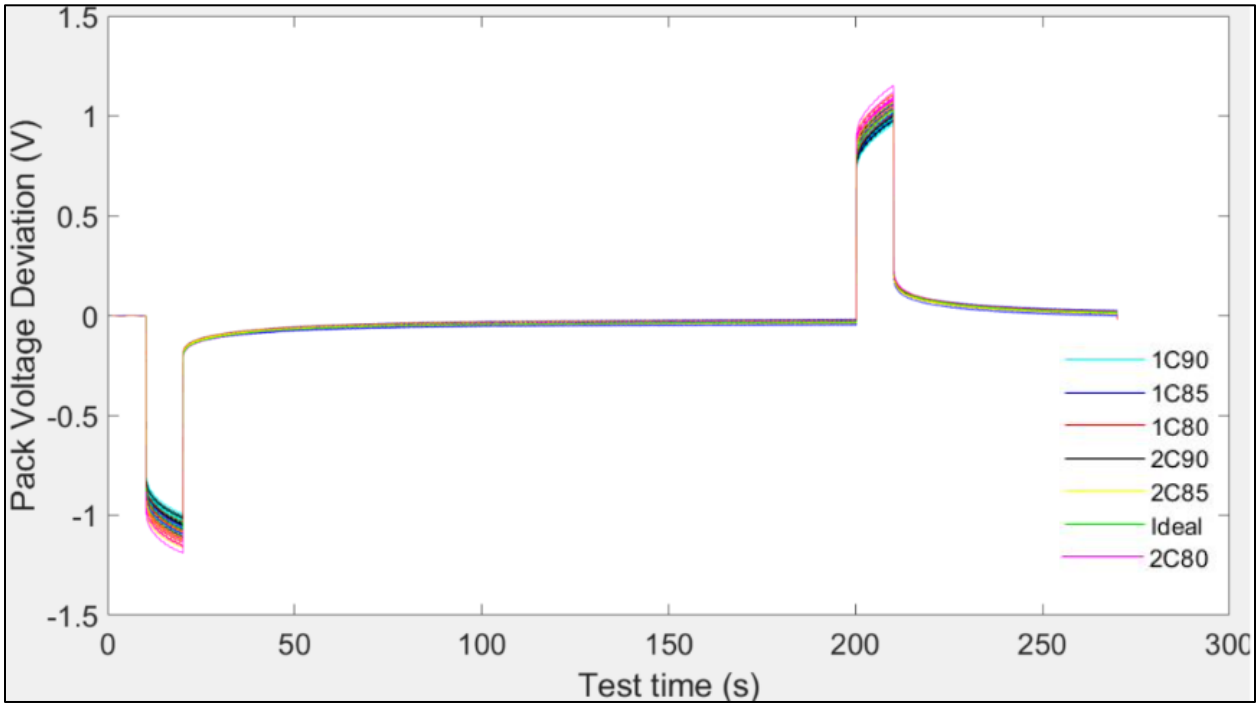

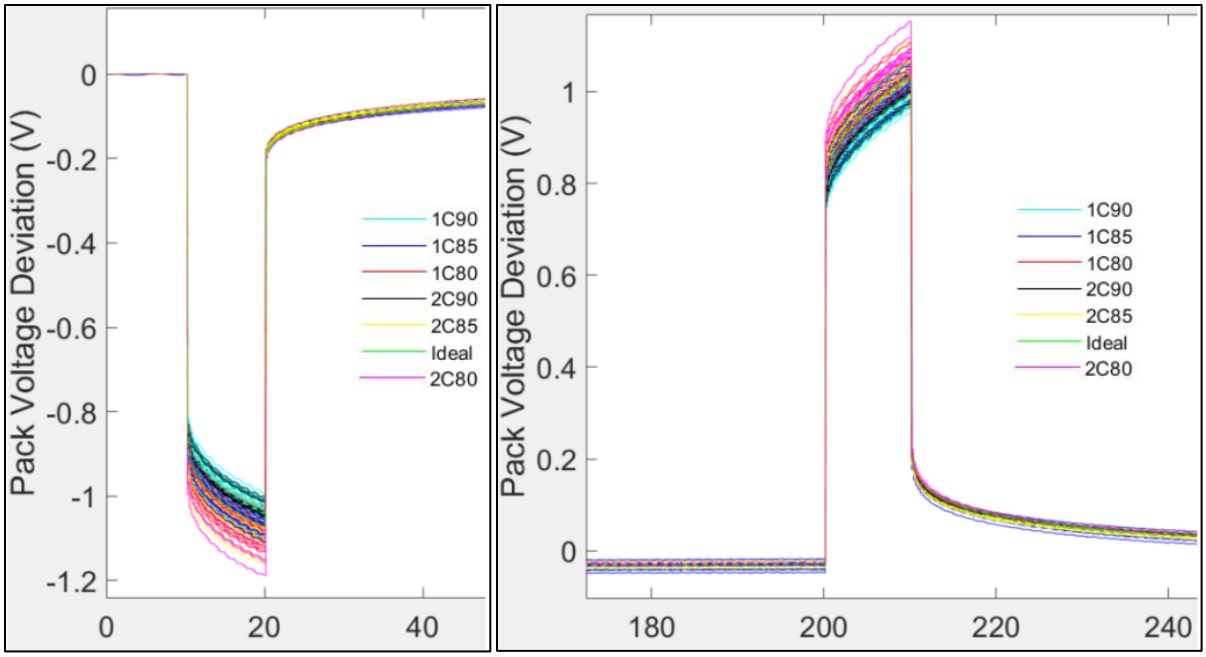

Figure 29: Final Pulse test for LFP packs - Raw results: Top – full test duration, Bottom left – expanded view of discharge pulse (x-axis – test time) and Bottom right – expanded view of charge pulse (x-axis – test time)

Again, as was the case with the NMC packs, the greatest voltage response was shown by the 2C80 cells as expected, while the remaining packs were more or less mixed with each other and hard to distinguish visually. Another point to note was that there is a much larger variation in response overall when it comes to the NMC packs compared to the LFP packs. This could again be attributed to the fact that the slope of the OCV-SoC curve is steeper for NMC cells compared to LFP cells as showcased in section 2.1, and the effect only compounds when a pack of 4 cells connected in series is formed. The three data analysis parameters used in section were applied to these tests as well and the correlation coefficient and their corresponding p-values are shown in the table below:

Table 14: Correlation Coefficients and p-values for Total SoH v/s DCIR, RMSD, MAPD

Relation	Correlation Coefficient	p-value
Total SoH ~ DCIR	-0.7379	2.95E-18
Total SoH ~ RMSD	-0.5837	2.28E-10
Total SoH ~ MAPD	-0.0592	0.5605

It was observed from the table that the high p-value along with a nearly zero correlation coefficient for the Total SoH ~ MAPD implies that there is no statistical significance for this relationship at all. However, the low p-values for both RMSD and DCIR relationships implied there was scope for SoH prediction with the inference from these parameters. In particular, the correlation coefficient of -0.73 was considerably higher than that for RMSD, coupled with a p-value several orders of magnitude lower, which promised a much better prediction potential. The plot of Total SoH ~ RMSD, MAPE and DCIR is shown below for visual reference:

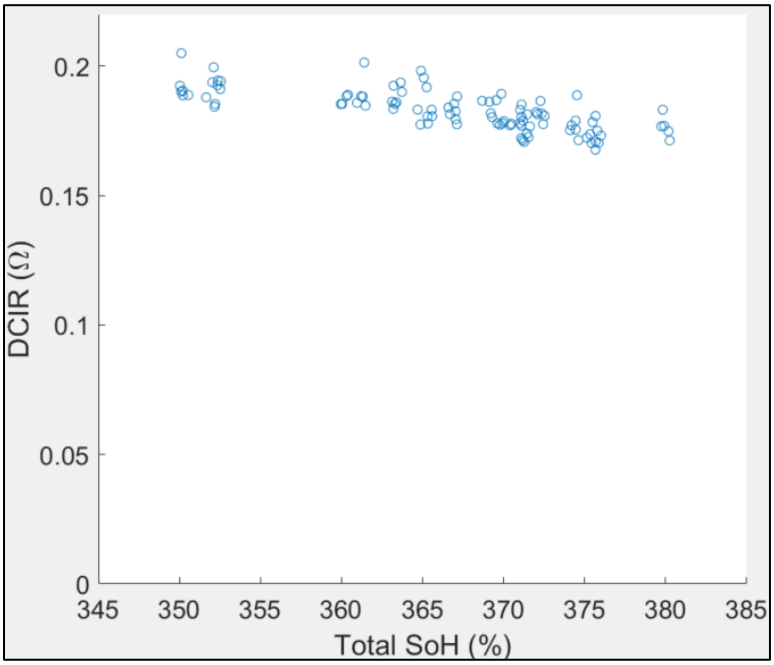

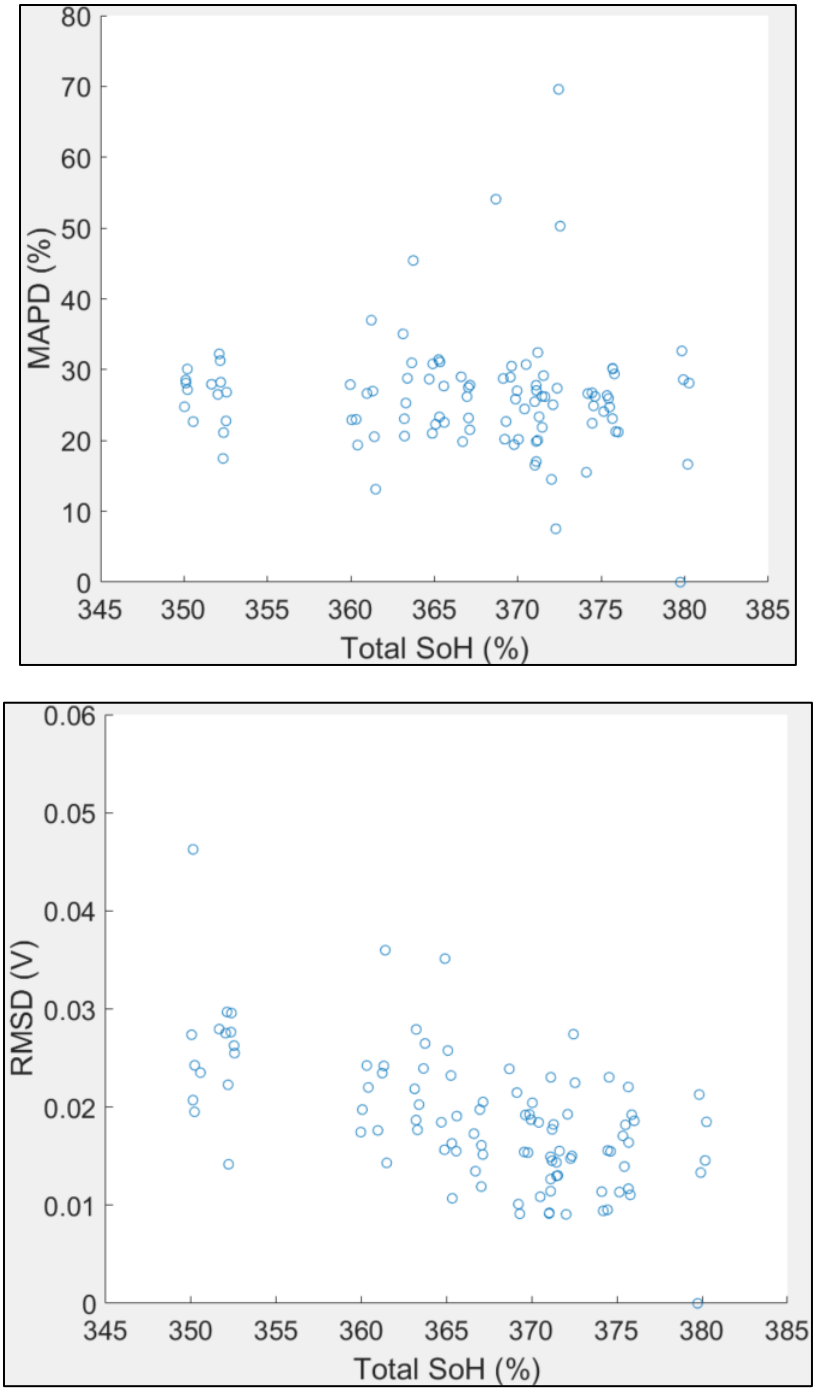

Figure 30: DCIR v/s Total SoH % for 99 LFP pack tests

From fig. 30, a relationship between the Total SoH and DCIR derived from the pulse tests was weak but does exist. However, it may not be as accurate as the modeling for the NMC cells as we can infer upon comparison with fig 28.

To summarize, it was observed that in case of the NMC packs, the best relationship observed was the Total SoH ~ MAPE relationship which seemed to be a linear one, while the RMSD and DCIR relationships were weaker. In contrast, for the LFP packs it was found that all three relationships were weak, but the Total SoH ~ DCIR term showed the most promise and again tended to a linear relationship.

4.4 Linear Modeling

For the next stage of modeling, the consideration that the nature of the Total SoH versus DCIR and MAPD generally tending toward a linear relationship prompted the proposal of a linear model for estimation of Total SoH. For this reason, a linear model with the formulation stated below was proposed:

$$Total\ SoH = \sum_{i=m}^{n} a_i V_i + K \qquad \textbf{Eq. 2}$$

Where total SoH is a linear combination of voltage responses (deviations from starting voltage) at different time steps of the pulse testing. a_i represents the coefficients of the equation at time steps corresponding to the *'i^{th}'* second in the test while V_i represents the voltage response of the given pack at the *'i^{th}'* second in the test. *K* is the intercept of the equation. Note that *'i'* varies from *m* through *n* and that *m* and *n* may not necessarily be from the start of the test to the end of the test.

4.4.1 Manipulation of data for linear model:

As mentioned earlier in section 3.1, the Arbin Battery Tester recorded voltage of the battery packs at a sampling rate of 100Hz or every 10ms, however, there was almost always a deviation in the exact time down to the millisecond at which the data was recorded which from test to test. Note that this does not necessarily refer to the time uncertainty from the Arbin, but the fact that the equipment itself did not measure the voltage response at the exact same time step for all the tests i.e., there was a time shift in the measurements. This issue was bypassed for the DCIR, RMSD and MAPD analysis as follows: Each recorded timestep in every step would be rounded to the nearest 10ms. An ideal test was considered as the reference test for each DCIR, RMSD and MAPD calculation. Every other test also has all its time steps also rounded to the nearest 10ms. So, the voltages corresponding to those rounded timesteps from each test were considered in the final calculations of the three parameters.

When it came to the linear model to establish a direct relationship between the measured pack voltage and the Total SoH, such an exercise was done slightly differently. Each timestep closest to a given second along the test duration was rounded to the corresponding second in the test. The corresponding voltage was recorded. As the tests were 270 seconds long, there were 270 pack voltage data points for every test, with each data point corresponding to each of the 270 seconds of the test. In effect, this was equivalent to sampling at 1Hz, but the tests were already conducted at a sampling rate of 100Hz, which is why this rounding exercise was needed.

Upon modifying the data from the tests in the described manner, the plot of the pack voltage deviation vs test time looked as follows in fig. 31:

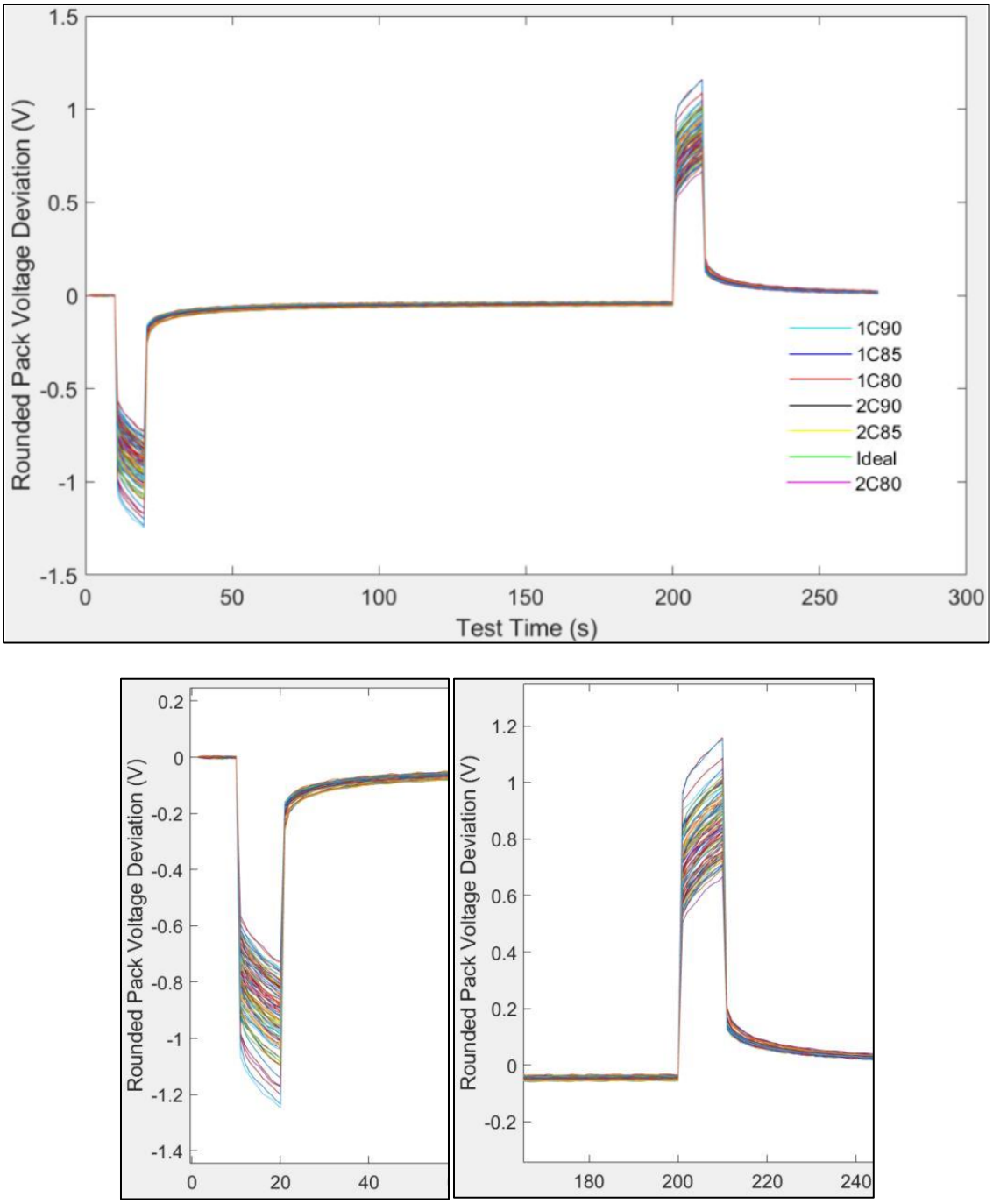

Figure 31: Rounded Test Data Plot - NMC packs: Top – full test duration, Bottom left – expanded view of discharge pulse (x-axis – test time) and Bottom right – expanded view of charge pulse (x-axis – test time)

When comparing fig. 31 to fig. 27 there was certainly some loss of information due to the effective sampling rate of 1Hz, but the general shape of the curves both during the pulse application as well as the rest periods were maintained. The corresponding curve for the LFP battery packs is shown in fig. 32 below:

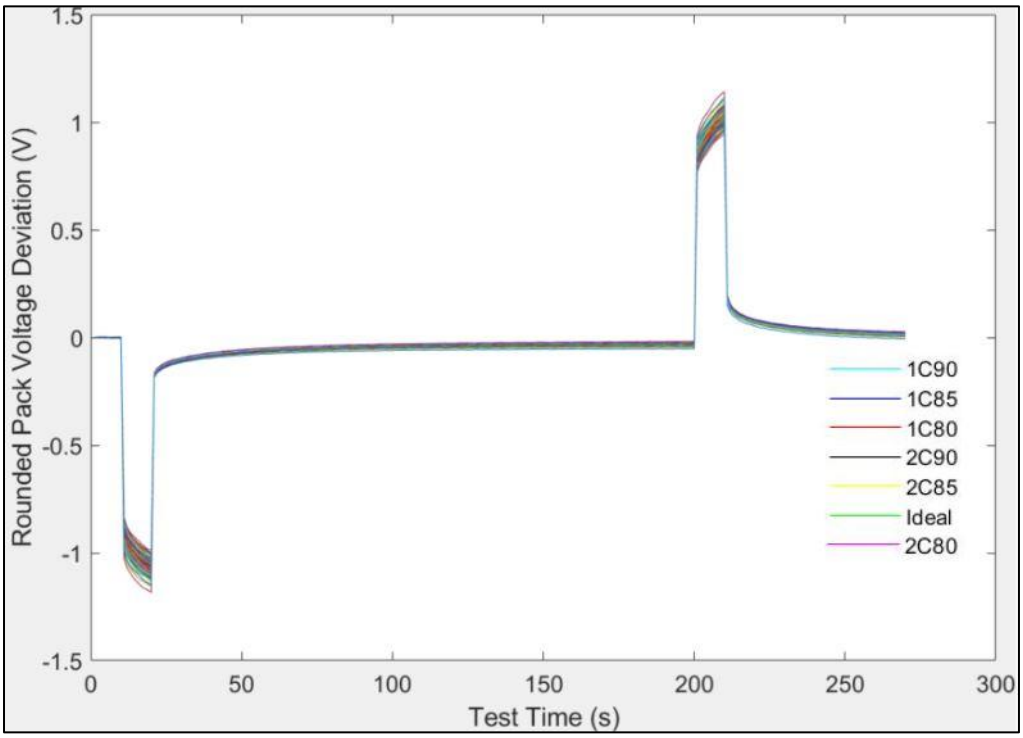

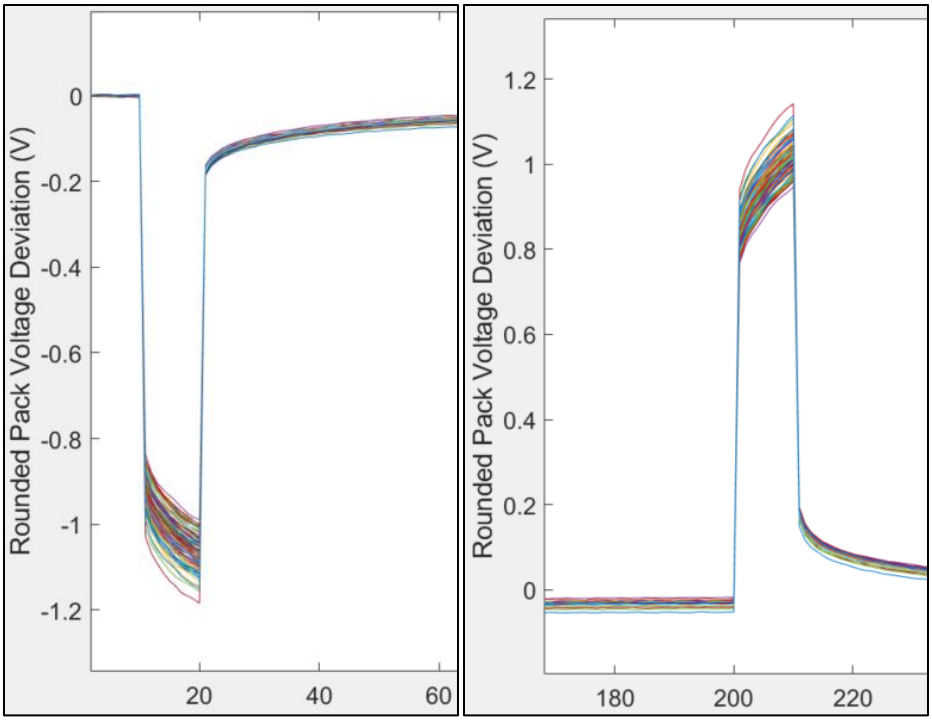

Figure 32: Rounded Test Data Plot - LFP packs: Top – full test duration, Bottom left – expanded view of discharge pulse (x-axis – test time) and Bottom right – expanded view of charge pulse (x-axis – test time)

Again, as was the case with the NMC battery packs, some loss of data due to effective sampling at 1Hz was observed, but the general shape of the curves was maintained for the pulse application and rest period.

4.4.2 The First Linear Model – NMC Chemistry:

The first linear model formulation that was analyzed was the one considering the 11 seconds measured from the start of each of charge and discharge pulse based on the notation from Eq. 2 is:

$$Total\ SoH = \sum_{i=m}^{n} a_i V_i + \sum_{i=p}^{q} a_i V_i + K \qquad \textbf{Eq. 3}$$

Where $m = 10$ and $n = 21$, corresponding to seconds 10 through 21 (discharge pulse). Similarly, $p = 200$ and $q = 211$, corresponding to seconds 200 through 211 (charge pulse). K represents the equation intercept.

When this model was applied to the 93 NMC tests, the following model parameters were generated by the R studio statistical computing software using the lm() - linear regression model:

Table 15: lm() model summary – First Linear Model - NMC chemistry

Coefficients	***Estimate (Std error)***	***t-value***	***p-value***
K (Intercept)	457.557 (3.717)	123.102	<**2.00E-16*****
a_{10}	30.593 (77.961)	0.392	0.69596
a_{11}	165.197 (170.623)	-0.968	0.33633
a_{12}	341.116 (220.314)	1.548	0.12612
a_{13}	268.928 (233.059)	-1.154	0.25252
a_{14}	110.708 (215.748)	0.513	0.6095
a_{15}	-42.138 (92.94)	-0.453	0.65169
a_{16}	68.468 (185.204)	0.37	0.71275
a_{17}	210.313 (183.677)	1.145	0.25616
a_{18}	297.595 (192.197)	-1.548	0.1261
a_{19}	29.972 (137.695)	0.218	0.82833
a_{20}	-9.022 (100.506)	-0.09	0.92873
a_{21}	434.944 (126.645)	3.434	**0.00101****
a_{200}	-170.012 (84.935)	-2.002	**0.04925***
a_{201}	239.53 (169.544)	1.413	0.16221
a_{202}	-23.977 (193.24)	-0.124	0.90161
a_{203}	86.573 (180.079)	0.481	0.63221
a_{204}	-43.714 (82.985)	-0.527	0.60004

a_{205}	-31.717 (165.761)	-0.191	0.84882
a_{206}	67.06 (185.068)	0.362	0.7182
a_{207}	-56.278 (188.768)	-0.298	0.7665
a_{208}	114.618 (163.378)	-0.702	0.48532
a_{209}	62.204 (115.486)	0.539	0.59187
a_{210}	-2.634 (126.409)	-0.021	0.98343
a_{211}	173.212 (148.525)	-1.166	0.24754

The overall model statistics were:

Overall Model Parameter	***Parameter Value (/w dof)***
Residual Standard Error	1.722 on 69 dof
Multiple R-squared	0.9696
Adjusted R-squared	0.9591
F-statistic	91.85 on 24 and 69 dof
p-value	<2.2e-16

The terms in the Coefficients portion of the model summary are defined as follows:

- The Estimate column denotes the values of the coefficients which the model has calculated.
- The standard error is a modified form of the standard deviation of the error associated with each coefficient. It is defined as:

$$S.E. = \frac{\sigma}{\sqrt{N}}$$

Where σ – standard deviation of given coefficient

N – number of samples, i.e., no. of tests

If *S.E. ($\hat{a}_i$)* is the standard error of a given coefficient and $\hat{a}_i$ is the estimated coefficient for voltage at the i^{th} second, then we can say with a 95% confidence interval that the true parameter a_i is given by $\hat{a}_i \pm 1.96 * S.E.\ (\hat{a}_i)$.

- The t-value is a measure of how many standard deviations our coefficient estimate is far away from the null hypothesis value for our coefficient of 0. The further away it is from 0, the higher likelihood that a relationship exists between the coefficient estimate and the total SoH, going against the null hypothesis. The t-value is defined as:

$$t - value = \frac{\hat{a}i}{S.E.(\hat{a}i)}$$

Where $\hat{a}_i$ - estimated coefficient for voltage at the i^{th} second

S.E. ($\hat{a}_i$) - the standard error of a given coefficient

- The p-value represents the probability of observing a coefficient value by random chance which is at least as extreme as the calculated coefficient $\hat{a}_i$. Therefore, the lower the p-value for the coefficient $\hat{a}_i$, the lower the probability of a relationship between the estimated coefficient and the Total SoH due to chance. To reject the null hypothesis that $\hat{a}_i = 0$, the standard p-value threshold of p-value<0.05 is used.

The inferences from the overall model performance metrics are as follows:

- The residual standard error is given by:

$$\hat{\sigma} = \sqrt{\frac{\sum_{i=1}^{N} \hat{\epsilon}_i^2}{N - p}}$$

Where $\hat{\epsilon}_i$ - Estimation error of the Total SoH of the i^{th} test,

N – number of tests

p – number of coefficients estimated

which effectively provides the standard deviation of the residuals, considering the number of parameters estimated.

- R^2 tells what proportion of the variance is explained by the model, and is given by

$$R^2 = 1 - \frac{\sum_{i=1}^{N} \hat{\epsilon}_i^2}{\sum_{i=1}^{N} (y_i - \bar{y})^2}$$

Where $\hat{\epsilon}_i$ - Estimation error of the Total SoH of the i^{th} test,

y_i – Total SoH estimate of the i^{th} test

$\bar{y}$ – mean value of all actual Total SoH

- The Adjusted R-squared addresses the increase in R^2 spuriously due to the addition of features (coefficients), and is given by

$$\bar{R}^2 = 1 - (1 - R^2)\frac{N - 1}{N - p - 1}$$

Where N – number of tests

p - number of coefficients estimated

Therefore, as the number of coefficients p increases, the required R^2 needed will increase as well to maintain the same adjusted R^2 value. Hence it is more appropriate to use in this case over the Multiple R-squared as it considers the effect of having multiple variables in the model. The closer the Adjusted R-Squared is to 1 the better the model.

- The F-statistic is used to confirm whether a group of variables are statistically significant in prediction of the response variable. In this case the group of variables would be the coefficients of the voltage and the response variable the Total SoH. The F-statistic is mathematically defined as,

$$F - Statistic = \frac{\sum_{i=1}^{N} (y_i - \bar{y})^2 / p}{\sum_{i=1}^{N} \hat{\epsilon}_i^2 / N - p - 1}$$

Where $\hat{\epsilon}_i$ - Estimation error of the Total SoH of the i^{th} test,

y_i – Total SoH estimate of the i^{th} test

$\bar{y}$ – mean value of all actual Total SoH

N – number of tests

p - number of coefficients estimated

The greater the F-statistic compared to unity, the greater the possibility of rejecting the null hypothesis of all coefficients being 0.

- The p-value is the probability of observing a sample outcome under the null hypothesis H_0, which is at least as extreme as the observed value. Therefore, the smaller the p-value, the more extreme the outcome and the stronger the evidence against H_0 and in favor of the proposed model.

In the generated linear model, it was observed that there was high statistical significance for the intercept, a_{21} and a_{200}, indicating that the response one second after the removal of the discharge current pulse and the application of the charge pulse hold the most significant data in predicting the Total SoH of a given pack. Furthermore, a high Adjusted R-squared of around 0.95 coupled with a high F-statistic of around 91 along with an extremely low p-value of the order of magnitude of 10^{-16} all of which when considered together point to a highly effective model in predicting the total SoH of an NMC pack.

In order to get the estimate of the confidence intervals of the predictions of the model, it was assumed that the errors take the shape of a normal distribution, which is based on the Central Limit Theorem. For sample sizes > 30, the z-distribution is commonly assumed, and the following formulation was used:

$$Prediction\ range = \hat{y} \pm Standard\ Error\ (S.E.) \times Z - score(C.I.)$$

Where $\hat{y}$ – Total SoH estimate from the model

A 95% confidence interval corresponds to a Z-score of 1.959. Therefore, for the given model having a S.E. = 1.799, the prediction range lies between:

$$\hat{y} \pm 1.799 \times 1.959 \Rightarrow \hat{y} \pm 3.524\ Total\ SoH\ \%\ points$$

Next, in order to demonstrate that the model structure was effective and would work on unseen data, a k-fold cross validation of the model was performed, and the performance of the model was assessed. A k-fold cross validation involves compartmentalizing the total number of tests into 'k' number of bins. Next, the model was trained on k-1 bins and evaluate its predictions of the total SoH on the one remaining bin. We select k = 3 in this evaluation since as it is commonly used in modeling efforts, ensuring that the model is trained on 2/3rds of the number of tests and validated on 1/3rd of the tests. Schematically, the 3-fold cross validation method looks as follows:

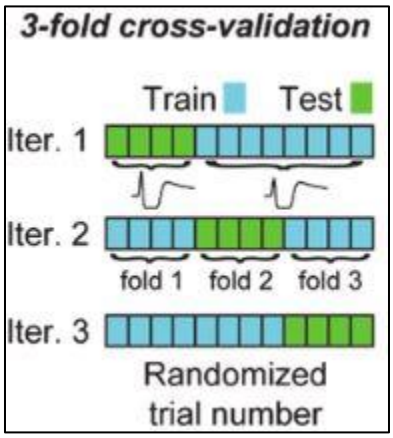

Figure 33: 3-fold cross validation schematic

The performance of the model is evaluated on three parameters. They are:

1. Root Mean Squared Error (RMSE) is the standard deviation of the residuals (prediction errors). It is given by

$$\text{RMSE} = \sqrt{\frac{\sum_{i=1}^{N}(Sact_i - Spr_i)^2}{N}}$$

Where $Sact_i$ - Actual total SoH of i^{th} pack

Spr_i - Predicted total SoH of i^{th} pack

N - number of tests

2. Mean Absolute Percentage Error (MAPE) is the average of the absolute percentage errors observed in the prediction of the total SoH. It is given by:

$$\text{MAPE} = \frac{1}{N} \sum_{i=1}^{N} \left| \frac{Sact_i - Spr_i}{Sact_i} \right| \times 100$$

Where $Sact_i$ - Actual total SoH of i^{th} pack

Spr_i - Predicted total SoH of i^{th} pack

N - number of tests

3. Mean Absolute Error (MAE) is the average magnitude of the errors in the set of total SoH predictions by the model. It is given by:

$$\text{MAE} = \frac{1}{N} \sum_{i=1}^{N} |Sact_i - Spr_i|$$

Where $Sact_i$ - Actual total SoH of i^{th} pack

Spr_i - Predicted total SoH of i^{th} pack

N - number of tests

In case of the 3-fold cross validation that was performed, the RMSE, MAPE and MAE was computed for each of the 3 folds, and then the average of the RMSE, MAPE and MAE obtained from the 3 testing bins is calculated. Since the process randomly selects tests from the nearly 100 tests, to ensure that there was no overfitting or bias, the 3-fold cross validation process was repeated 1,000 times, and the average of the RMSE, MAPE and MAE was taken. This ensured that the process was extensive, and that the model structure was valid for any data in the given total SoH ranges. The results of the 1,000 3-fold cross validation were as follows:

1. Mean RMSE = 2.24 Total SoH percentage points
2. Mean MAPE = 0.49% error in Total SoH prediction

3. Mean MAE = 1.78 Total SoH percentage points

The above three performance parameters taken together, along with the overall model statistics in section 4.3 show that this model structure was highly robust and effective in predicting the total SoH of a pack in case of the NMC chemistry.

4.4.3 The Second Linear Model – NMC Chemistry

Upon further iterations of the model structure, it was observed that an alternate model structure which only considered the first discharge pulse and not the second charge pulse, yielded a slightly better model. The modified model structure was as follows:

$$Total\ SoH = \sum_{i=m}^{n} a_i V_i + K \qquad \textbf{Eq. 4}$$

Where $m = 10$ and $n = 21$, corresponding to seconds 10 through 21 (discharge pulse). K represents the equation intercept.

When this model was applied to the 93 NMC tests, the following model parameters were generated by the R studio statistical computing software using the lm() - linear regression model:

Table 16: lm() model summary – Second Linear Model - NMC chemistry

Coefficients	***Estimate (Std Error)***	***t-value***	***p-value***
K (Intercept)	457.459 (3.497)	130.809	< 2e-16***
a_{10}	-42.065 (70.307)	-0.598	0.5513
a_{11}	-44.138 (155.205)	-0.284	0.7768
a_{12}	162.662 (205.624)	0.791	0.4312
a_{13}	-147.289 (221.906)	-0.664	0.5087
a_{14}	50.23 (213.016)	0.236	0.8142
a_{15}	-10.567 (90.379)	-0.117	0.9072
a_{16}	39.175 (192.237)	0.204	0.839

a_{17}	327.385 (177.362)	1.846	0.0686.
a_{18}	-290.039 (172.744)	-1.679	0.097.
a_{19}	-37.253 (127.282)	-0.293	0.7705
a_{20}	-124.291 (55.926)	-2.222	0.029*
a_{21}	668.497 (82.922)	8.062	5.68E-12***

The overall model statistics were:

Overall Model Parameter	***Parameter Value (/w dof)***
Residual Standard Error	1.833 on 81 dof
Multiple R-squared	0.9596
Adjusted R-squared	0.9537
F-statistic	160.5 on 12 and 81 dof
p-value	<2.2e-16

From the model summary, the intercept, coefficients a_{20} and a_{21} had significant statistical significance based on their t-values and p-values. The Adjusted R-squared was marginally lower but the F-statistic was much higher than the previously proposed model structure. The p-value remained at the same order of magnitude. Next, the 3-fold cross validation was performed and the average RMSE, MAPE and MAE over 1,000 iterations were calculated. The prediction range was again evaluated based on the z-distribution as follows:

$$Prediction\ range = \hat{y} \pm Standard\ Error\ (S.E.) \times Z - score(C.I.)$$

Where $\hat{y}$ – Total SoH estimate from the model

A 95% confidence interval corresponds to a Z-score of 1.959. Therefore, for the given model having a S.E. = 1.833, the prediction range lies between:

$$\hat{y} \pm 1.833 \times 1.959 \Rightarrow \hat{y} \pm 3.590\ Total\ SoH\ \%\ points$$

The model performance results in comparison with the two-pulse model structure are shown below:

Table 17: Comparison between First and Second Linear Model – NMC Chemistry

	One Pulse Model (Second Linear Model)	**Two Pulse Model (First Linear Model)**
Mean RMSE	2.05 total SoH % points	2.24 total SoH % points
Mean MAPE	0.43% error in total SoH prediction	0.49% error in total SoH prediction
Mean MAE	1.60 total SoH % points	1.78 total SoH % points

There was a slight improvement in model performance based on all 3 evaluation parameters by only considering the first pulse in the tests. This had been determined after multiple iterations with various parts of the pulse and rest periods considered in the experiment and the best performance was observed when only the first pulse was considered in the model equation.

4.4.4 The First Linear Model – LFP Chemistry

In the case of LFP packs, a similar comparison between both the model structures was conducted. The first linear model formulation was by considering the 11 seconds measured from the start of each of charge and discharge pulse:

$$Total\ SoH = \sum_{i=m}^{n} a_i V_i + \sum_{i=p}^{q} a_i V_i + K \qquad \textbf{Eq. 5}$$

Where $m = 10$ and $n = 21$, corresponding to seconds 10 through 21 (discharge pulse). Similarly, $p = 200$ and $q = 211$, corresponding to seconds 200 through 211 (charge pulse). K represents the equation intercept.

When this model was applied to the 99 LFP tests, the following model parameters were generated by the R studio statistical computing software using the lm() - linear regression model:

Table 18: lm() model summary – First Linear Model – LFP chemistry

Coefficients	***Estimate (Std Error)***	***t-value***	***p-value***
K (Intercept)	475.72 (49.15)	9.678	7.72E-15***
a_{10}	5.07 (466.06)	0.011	0.9913
a_{11}	-125.5 (761.54)	-0.165	0.8695
a_{12}	831.21 (714.5)	1.163	0.2484
a_{13}	-1186.37 (699.24)	-1.697	0.0939.
a_{14}	862.75 (663.82)	1.3	0.1977
a_{15}	-477.01 (301.43)	-1.582	0.1177
a_{16}	74.02 (605.85)	0.122	0.9031
a_{17}	-25.36 (742.52)	-0.034	0.9728
a_{18}	-794.95 (715.91)	-1.11	0.0000
a_{19}	941.38 (580.6)	1.621	0.1091
a_{20}	1442.33 (839.81)	1.717	0.09.
a_{21}	-2433.83 (1053.44)	-2.31	0.0236*
a_{200}	350.37 (492.9)	0.711	0.4794
a_{201}	628.38 (654.29)	0.96	0.3399
a_{202}	-133.58 (653.04)	-0.205	0.8385

a_{203}	963.74 (552.03)	1.746	0.0849.
a_{204}	-94.11 (251.33)	-0.374	0.7091
a_{205}	-160.13 (520.52)	-0.308	0.7592
a_{206}	-501.1 (602.77)	-0.831	0.4084
a_{207}	-104.09 (684.36)	-0.152	0.8795
a_{208}	-633.63 (602.55)	-1.052	0.2964
a_{209}	-380.92 (413.25)	-0.922	0.3596
a_{210}	254.61 (770.15)	0.331	0.7419
a_{211}	635.88 (918.46)	0.692	0.4909

The overall model statistics were:

Overall Model Parameter	***Parameter Value (/w dof)***
Residual Standard Error	5.441 on 75 dof
Multiple R-squared	0.6685
Adjusted R-squared	0.5624
F-statistic	6.301 on 24 and 75 dof
p-value	3.71E-10

The intercept (K) and coefficient a_{21} were statistically significant in predicting the total SoH based on the t-value and p-value, however, the overall model performance was much less satisfactory than the NMC models. Adjusted R-squared of ~0.56 and F-statistic being nearly two orders of magnitude lower than the NMC model indicated a much less accurate prediction capability. The p-value of order of magnitude of 10^{-10} did however still indicate that there was still an extremely

low probability of there being a relationship between the coefficients and Total SoH by random chance. The prediction range was again evaluated based on the z-distribution as follows:

$$Prediction\ range = \hat{y} \pm Standard\ Error\ (S.E.) \times Z - score(C.I.)$$

Where $\hat{y}$ – Total SoH estimate from the model

A 95% confidence interval corresponds to a Z-score of 1.959. Therefore, for the given model having a S.E. = 5.441, the prediction range lies between:

$$\hat{y} \pm 5.441 \times 1.959 \Rightarrow \hat{y} \pm 10.658\ Total\ SoH\ \%\ points$$

The model's performance based on the 3-fold cross validation averaged over 1,000 iterations was as follows:

1. Mean RMSE = 6.99 Total SoH percentage points
2. Mean MAPE = 1.55% error in Total SoH prediction
3. Mean MAE = 5.66 Total SoH percentage points

This confirmed that the performance was significantly poorer compared to the NMC models.

4.4.5 The Second Linear Model – LFP Chemistry

However, it was again noted that when only the first pulse was considered in the model, the performance slightly improved. The one pulse model structure is again described as follows:

$$Total\ SoH = \sum_{i=m}^{n} a_i V_i + K \qquad \textbf{Eq. 6}$$

Where $m = 10$ and $n = 21$, corresponding to seconds 10 through 21 (discharge pulse). K represents the equation intercept.

When this model was applied to the 93 NMC tests, the following model parameters were generated by the R studio statistical computing software using the lm() - linear regression model:

Table 19: lm() model summary – Second Linear Model – LFP chemistry

Coefficients	***Estimate (Std error)***	***t-value***	***p-value***
K (Intercept)	531.463 (29.867)	17.795	<2e-16***
a_{10}	163.911 (430.061)	0.381	0.704
a_{11}	31.227 (647.269)	0.048	0.9616
a_{12}	800.569 (660.95)	1.211	0.2291
a_{13}	-890.221 (660.429)	-1.348	0.1812
a_{14}	1071.882 (587.028)	1.826	0.0713.
a_{15}	-611.989 (291.153)	-2.102	0.0384*
a_{16}	-73.342 (589.659)	-0.124	0.9013
a_{17}	-6.764 (718.413)	-0.009	0.9925
a_{18}	-831.47 (707.814)	-1.175	0.2433
a_{19}	469.378 (527.705)	0.889	0.3762
a_{20}	1703.903 (759.528)	2.243	0.0274*
a_{21}	1320.177 (884.415)	-1.493	0.1391

The overall model statistics were:

Overall Model Parameter	***Parameter Value (/w dof)***
Residual Standard Error	5.459 on 87 dof
Multiple R-squared	0.6128
Adjusted R-squared	0.5594
F-statistic	11.48 on 12 and 87 dof
p-value	1.98E-13

It was seen that the intercept (*K*), coefficients a_{15} and a_{20} were statistically significant in the model predicting the total SoH of the LFP battery pack. The Adjusted R-squared of 0.5594 was slightly worse than the previous model which considered both pulses, however the F-statistic at 11.48 was substantially better. The p-value was also better at 3 orders of magnitude lower.

The prediction range was again evaluated based on the z-distribution as follows:

$$Prediction\ range = \hat{y} \pm Standard\ Error\ (S.E.) \times Z - score(C.I.)$$

Where $\hat{y}$ – Total SoH estimate from the model

A 95% confidence interval corresponds to a Z-score of 1.959. Therefore, for the given model having a S.E. = 5.459, the prediction range lies between:

$$\hat{y} \pm 5.459 \times 1.959 \Rightarrow \hat{y} \pm 10.694\ Total\ SoH\ \%\ points$$

Next, the 3-fold cross validation was performed and the average of the RMSE, MAPE and MAE over 1,000 iterations were computed. The model performance results in comparison with the two-pulse model structure are shown as follows:

Table 20: Comparison between First and Second Linear Model – LFP Chemistry

	One Pulse Model (First Pulse Only)	**Two Pulse Model**
Mean RMSE	6.09 total SoH % points	6.99 total SoH % points
Mean MAPE	1.32% error in total SoH prediction	1.55% error in total SoH prediction
Mean MAE	4.81 total SoH % points	5.66 total SoH % points

There was a considerable improvement in the model performance when only the first pulse was considered in the model. However, the overall performance was still substantially worse as compared to the NMC battery pack models. The comparison of the best models for the NMC and LFP cells is shown in the following table for reference:

Table 21: Comparison between NMC and LFP Second Linear Models (One Pulse Models)

	NMC Second Linear Model (One Pulse only)	**LFP Second Linear Model (One Pulse only)**
Mean RMSE	2.05 total SoH % points	6.09 total SoH % points
Mean MAPE	0.43% error in total SoH prediction	1.32% error in total SoH prediction
Mean MAE	1.60 total SoH % points	4.81 total SoH % points

The hypothesis as to why the NMC models were far more accurate leads back to the OCV-SoC curves for the two chemistries. From figure 12, the steeper OCV-SoC curve in case of the NMC cells (6.4mV/%SoC) as opposed to the LFP cells (1.4mV/%SoC) over the 15%-85% SoC range possibly induces a greater discernible response to pulse testing. Every time a current pulse was passed, for the same reduction in SoC, there was a greater change in the OCV of the NMC cells as compared to the LFP cells. Therefore, when there was a difference in the SoH of cells within a pack, a given current pulse induced a different change in SoC for each cell within the pack.

The OCV change and hence the voltage response due to this is always expected to be greater for NMC cells as compared to LFP cells. This deviation becomes exaggerated when these

cells are connected in series to form their respective packs. One solution to this issue could potentially be using voltage measurement instruments with higher sensitivity to discern two packs of LFP chemistry with different Total SoH. This would involve additional analysis of the instrument sensitivity to determine the appropriate level of instrument sensitivity which would be needed to detect the difference between two LFP packs of different Total SoH and is suggested as part of future work in chapter 5.

Amongst the various currently available commercial Lithium-ion battery chemistries, the lowest slope is that of the LFP cells followed by Lithium Titanium Oxide (LTO) cells [27]. All the other major commercial chemistries ranging from Lithium-Manganese-Oxide (LMO), Lithium-Cobalt-Oxide (LCO), and Nickel-Cobalt-Aluminum-Oxide (NCA) have slopes comparable to that of the NMC chemistry of cells. This leads to the belief that since this thesis provides a proof of concept for successful Total SoH estimation of NMC battery packs, a similar accuracy may be expected for LMO, LCO and NCA chemistries as well, and the limiting case would likely be that of the LFP chemistry itself.

This concludes the discussion in chapter 4, where the final pulse test was introduced based on the findings in chapter 3, followed by the initial statistical analysis which led to the proposal of the linear model for estimation of the Total SoH of the packs. The R studio statistical computing software enabled the linear modeling and generated various parameters which were defined and compared for the NMC and LFP cells over the single pulse and both the pulses from the tests. It was found that the single pulse yielded slightly better models for both chemistries, but the LFP models were much less accurate regardless. A possible explanation was discussed for the same which concludes this chapter. Chapter 5 discusses the conclusion of this work and proposes recommendations for future work.

Chapter 5: Conclusion and Future Recommendations

Firstly, the potential applications of series connected Battery Pack SoH estimation were discussed. Next, the complexities involved in the degradation of individual cells, along with the additional factors such as inconsistencies which come into play when a series connected battery pack is made, were described. Single cell SoH estimation methods were broadly classified, and an overview of the literature was provided for Battery Pack SoH estimation.

Based on the overall literature review, two key research gaps were identified, namely the lack of empirical models which measure only the pack voltages, and lack of rapid estimation techniques involving just the pack voltages as model inputs. A short pulse test was proposed as part of a rapid Battery Pack SoH estimation technique, and as a proof of concept, around 14 cells each of NMC and LFP chemistries were degraded to predefined SoH in order to create a variety of battery packs with different SoH.

A set of preliminary tests were carried out to ascertain the correlation between pulse magnitude and duration, based on which a final pulse test was devised. The final pulse test is simple and includes just two 2C, 10 second charge and discharge pulses. A simple linear model that takes in the measured pack voltages at particular time steps during the test, is accurately able to estimate the Total SoH of the Battery Pack. For NMC cells, an RMSE of 2.05 Total SoH % points and MAE of 1.60 Total SoH % points. However, the LFP chemistry of cells only achieve an RMSE of 6.09 Total SoH % points and MAE of 4.80 Total SoH % points.

It is hypothesized that this performance differential exists due to the much steeper OCV-SoC curve for NMC cells over LFP cells. It is also noteworthy that when only the timesteps corresponding to the first discharge pulse were fed to the model, it gave a slightly improved performance.

Overall, the modeling effort serves as a proof of concept for rapid estimation of SoH of a given series connected battery pack, especially for the NMC chemistry. Furthermore, since a simple empirical model was used, it also shows that a limited dataset, without the complexities of accurately estimating >32 model parameters in physics-based modeling, is sufficient for rapid estimation of battery pack SoH. The quick nature of the test also opens the possibility of it being used for periodic diagnostics efforts as well in EV and ESS applications where time constraints for maintenance could be an important consideration. Nonetheless, there are further improvements which can be made to the modeling to provide added utility and further key information of the status of a series connected battery pack. Some key recommendations for future work are as follows:

1. Inclusion of instrument sensitivity analysis in conjunction with uncertainty analysis as part of the overall model accuracy assessment can potentially also help determine the level of instrumentation required to perform the pulse tests needed for the SoH estimation. This would determine if the LFP chemistry battery pack Total SoH estimation is feasible, and if so, with what accuracy. Furthermore, this can also determine if the existing test setups in the BMS of current EVs as well as in ESS are sufficient for accurate modeling or if upgraded instruments may be needed based on battery chemistry.
2. An expansion of the total SoH range in the modeling is recommended. Currently only the total SoH ranging from 350% to 380% are part of the model, with limited combinations. This can be expanded to say, 320% to 380% total SoH when all possible variations of SoH using the degraded cells are employed.
3. Tests with the cells balanced at different SoCs can also be explored, especially along parts of the OCV-SoC curves where the slope is steep. Even though balancing is not particularly

common at low SoCs, there is a possibility of generating a more accurate model based simply on the steepness of the curves, which is worth exploring.

4. An additional parameter, such as the standard deviation of the cell SoH distribution within a pack may also yield more information about a given series connected battery pack. This will almost certainly require more complex models, but the information can prove to be quite useful in both battery pack diagnostics and 2nd life ESS applications.
5. With further testing, it may be possible to collect sufficient data to also generate a Machine Learning model for battery pack SoH estimation and compare its results with the model proposed in this thesis.

It is also noteworthy that as of the submission of this thesis, there is work currently underway in trying to address many of the recommendations at the UC Davis Green Technology Laboratory.

Chapter 6: References

[1] Marques, P., Garcia, R., Kulay, L., and Freire, F., 2019, "Comparative Life Cycle Assessment of Lithium-Ion Batteries for Electric Vehicles Addressing Capacity Fade," Journal of Cleaner Production, **229**.

[2] Yao, L., Xu, S., Tang, A., Zhou, F., Hou, J., Xiao, Y., and Fu, Z., 2021, "A Review of Lithium-Ion Battery State of Health Estimation and Prediction Methods," World Electric Vehicle Journal 2021, Vol. 12, Page 113, **12**(3), p. 113.

[3] Edge, J. S., O'Kane, S., Prosser, R., Kirkaldy, N. D., Patel, A. N., Hales, A., Ghosh, A., Ai, W., Chen, J., Yang, J., Li, S., Pang, M. C., Bravo Diaz, L., Tomaszewska, A., Marzook, M. W., Radhakrishnan, K. N., Wang, H., Patel, Y., Wu, B., and Offer, G. J., 2021, "Lithium Ion Battery Degradation: What You Need to Know," Physical Chemistry Chemical Physics, **23**(14).

[4] Birkl, C. R., Roberts, M. R., McTurk, E., Bruce, P. G., and Howey, D. A., 2017, "Degradation Diagnostics for Lithium Ion Cells," Journal of Power Sources, **341**.

[5] Lagnoni, M., Nicolella, C., and Bertei, A., 2021, "Survey and Sensitivity Analysis of Critical Parameters in Lithium-Ion Battery Thermo-Electrochemical Modeling," Electrochimica Acta, **394**.

[6] Barzacchi, L., Lagnoni, M., Rienzo, R. di, Bertei, A., and Baronti, F., 2022, "Enabling Early Detection of Lithium-Ion Battery Degradation by Linking Electrochemical Properties to Equivalent Circuit Model Parameters," Journal of Energy Storage, **50**.

[7] Ahmed, R., Gazzarri, J., Onori, S., Habibi, S., Jackey, R., Rzemien, K., Tjong, J., and Lesage, J., 2015, "Model-Based Parameter Identification of Healthy and Aged Li-Ion

Batteries for Electric Vehicle Applications," SAE International Journal of Alternative Powertrains, **4**(2).

[8] Hu, X., Feng, F., Liu, K., Zhang, L., Xie, J., and Liu, B., 2019, "State Estimation for Advanced Battery Management: Key Challenges and Future Trends," Renewable and Sustainable Energy Reviews, **114**.

[9] Hoque, M. A., Nurmi, P., Kumar, A., Varjonen, S., Song, J., Pecht, M. G., and Tarkoma, S., 2021, "Data Driven Analysis of Lithium-Ion Battery Internal Resistance towards Reliable State of Health Prediction," Journal of Power Sources, **513**.

[10] Che, Y., Deng, Z., Tang, X., Lin, X., Nie, X., and Hu, X., 2022, "Lifetime and Aging Degradation Prognostics for Lithium-Ion Battery Packs Based on a Cell to Pack Method," Chinese Journal of Mechanical Engineering (English Edition), **35**(1).

[11] Zhang, C., Jiang, Y., Jiang, J., Cheng, G., Diao, W., and Zhang, W., 2017, "Study on Battery Pack Consistency Evolutions and Equilibrium Diagnosis for Serial- Connected Lithium-Ion Batteries," Applied Energy, **207**.

[12] Jiang, Y., Jiang, J., Zhang, C., Zhang, W., Gao, Y., and Mi, C., 2019, "A Copula-Based Battery Pack Consistency Modeling Method and Its Application on the Energy Utilization Efficiency Estimation," Energy, **189**.

[13] Das, U. K., Shrivastava, P., Tey, K. S., bin Idris, M. Y. I., Mekhilef, S., Jamei, E., Seyedmahmoudian, M., and Stojcevski, A., 2020, "Advancement of Lithium-Ion Battery Cells Voltage Equalization Techniques: A Review," Renewable and Sustainable Energy Reviews, **134**.

[14] Bi, J., Zhang, T., Yu, H., and Kang, Y., 2016, “State-of-Health Estimation of Lithium-Ion Battery Packs in Electric Vehicles Based on Genetic Resampling Particle Filter,” Applied Energy, **182**.

[15] Hua, Y., Cordoba-Arenas, A., Warner, N., and Rizzoni, G., 2015, “A Multi Time-Scale State-of-Charge and State-of-Health Estimation Framework Using Nonlinear Predictive Filter for Lithium-Ion Battery Pack with Passive Balance Control,” Journal of Power Sources, **280**.

[16] Cordoba-Arenas, A., Onori, S., and Rizzoni, G., 2015, “A Control-Oriented Lithium-Ion Battery Pack Model for Plug-in Hybrid Electric Vehicle Cycle-Life Studies and System Design with Consideration of Health Management,” Journal of Power Sources, **279**.

[17] Diao, W., Jiang, J., Zhang, C., Liang, H., and Pecht, M., 2017, “Energy State of Health Estimation for Battery Packs Based on the Degradation and Inconsistency,” *Energy Procedia*.

[18] Yu, H., Li, J., Ji, Y., and Pecht, M., 2022, “Life-Cycle Parameter Identification Method of an Electrochemical Model for Lithium-Ion Battery Pack,” Journal of Energy Storage, **47**.

[19] Su, L., Wang, Z., and Ren, Y., 2019, “A Novel Two-Steps Method for Estimation of the Capacity Imbalance among in-Pack Cells,” Journal of Energy Storage, **26**.

[20] Song, L., Zhang, K., Liang, T., Han, X., and Zhang, Y., 2020, “Intelligent State of Health Estimation for Lithium-Ion Battery Pack Based on Big Data Analysis,” Journal of Energy Storage, **32**.

[21] Huotari, M., Arora, S., Malhi, A., and Främling, K., 2021, “Comparing Seven Methods for State-of-Health Time Series Prediction for the Lithium-Ion Battery Packs of Forklifts,” Applied Soft Computing, **111**.

[22] Love, C. T., Virji, M. B. V., Rocheleau, R. E., and Swider-Lyons, K. E., 2014, "State-of-Health Monitoring of 18650 4S Packs with a Single-Point Impedance Diagnostic," Journal of Power Sources, **266**.

[23] Song, Y., Liu, D., and Peng, Y., 2019, "Series-Connected Lithium-Ion Battery Pack Health Modeling with Cell Inconsistency Evaluation," *I2MTC 2019 - 2019 IEEE International Instrumentation and Measurement Technology Conference, Proceedings*.

[24] Xu, J., Mei, X., Wang, X., Fu, Y., Zhao, Y., and Wang, J., 2021, "A Relative State of Health Estimation Method Based on Wavelet Analysis for Lithium-Ion Battery Cells," IEEE Transactions on Industrial Electronics, **68**(8).

[25] Yang, S., Zhang, C., Jiang, J., Zhang, W., Zhang, L., and Wang, Y., 2021, "Review on State-of-Health of Lithium-Ion Batteries: Characterizations, Estimations and Applications," Journal of Cleaner Production, **314**.

[26] Ding, Y., Cano, Z. P., Yu, A., Lu, J., and Chen, Z., 2019, "Automotive Li-Ion Batteries: Current Status and Future Perspectives," Electrochemical Energy Reviews, **2**(1).

[27] Yu, Q. Q., Xiong, R., Wang, L. Y., and Lin, C., 2018, "A Comparative Study on Open Circuit Voltage Models for Lithium-Ion Batteries," Chinese Journal of Mechanical Engineering (English Edition), **31**(4).

[28] Li, Z., Shi, X., Shi, M., Wei, C., Di, F., and Sun, H., 2020, "Investigation on the Impact of the HPPC Profile on the Battery ECM Parameters' Offline Identification," *2020 Asia Energy and Electrical Engineering Symposium, AEEES 2020*.

Appendix

Appendix A: Specifications of TestEquity Temperature Chamber

The specifications of the TestEquity Temperature Chamber based on the manufacturer's brochure are as follows:

The Test Equity 1007C Temperature Chamber allows up to 256 steps to be programmed into as many as 40 namable profiles. The context sensitive information key and guided steps make profile programming fast and easy. A four-line backlit LCD displays programming, setup, operating and help information. A large LED readout indicates the actual chamber temperature with 0.1° resolution. Internal logic provides refrigeration compressor control for responsive and reliable performance. The Test Equity 1007C includes two alarms and seven event outputs to control remote devices. RS-232C communications is also included. GPIB, Ethernet and analog retransmit are available as options. Features and specifications of the 1007C Environmental Chamber include:

- -73°C to +175°C Temperature Range (opt. to +205°C)
- 7 Cu Ft Workspace, 24 W x 21 H x 24 D (198 Liters)
- Programmable Temperature Controller
- RS-232 Interface (Opt. GPIB and Ethernet)
- High/Low Limit Control and Alarm
- Viewing Window & Interior Light
- 4" Access Ports on Left & Right Side
- Non-CFC Cascade Refrigeration

Appendix B: Specifications of Prusa 3D Printer

The specifications of the Prusa Original i3 MK3S+ based on the manufacturer's brochure are as follows:

Build Volume	25×21×21 cm (9.84"×8.3"×8.3")
Layer height	0.05 - 0.35 mm
Nozzle	0.4mm default, wide range of other diameters/nozzles supported
Filament diameter	1.75 mm
Supported materials	Wide range of thermoplastics, including PLA, PETG, ASA, ABS, PC (Polycarbonate), CPE, PVA/BVOH, PVB, HIPS, PP (Polypropylene), Flex, nGen, Nylon, Carbon filled, Woodfill and other filled materials.
Max travel speed	200+ mm/s
Max nozzle temperature	300 °C / 572 °F
Max heatbed temperature	120 °C / 248 °F
Extruder	Direct Drive, Bondtech gears, E3D V6 hotend
Print surface	Removable magnetic steel sheets (*) with different surface finishes, heatbed with cold corners compensation
Printer dimensions (without spool)	7 kg, 50×55×40 cm; 19.6×21.6×15.7 in (X×Y×Z)
Power consumption	PLA settings: 80W / ABS settings: 120W